inorganics

MDPI

Review

Reversibility as a Design Principle in Inorganic, Organometallic and Organic Redox Mediators for Biosensors

Angel A. J. Torriero

School of Life and Environmental Sciences, Faculty of Science, Engineering & Built Environment, Deakin University, Burwood, VIC 3125, Australia; angel.torriero@deakin.edu.au; Tel.: +61-3-9244-6897

Abstract

Redox mediators are central to electrochemical biosensors, enabling electron transfer between deeply buried enzymatic cofactors and electrode surfaces when direct electron transfer is kinetically inaccessible. Among all design parameters, the reversibility of mediator redox cycling remains the most decisive yet under-examined factor governing biosensor stability, drift and long-term reproducibility. This review establishes reversibility as a unifying framework grounded in inorganic and organometallic redox chemistry, with particular emphasis on coordination environments, ligand-field effects and outer-sphere electron-transfer pathways. Recent advances (2010–2025) in ruthenium and osmium polypyridyl complexes, cobalt macrocycles, hexacyanoferrates and Prussian Blue analogues are examined alongside ferrocene derivatives and other organometallic mediators, which together define the upper limits of reversible behaviour. Organic mediator families, including quinones, phenazines, indophenols, aminophenols and viologens, are discussed as mechanistic contrasts that highlight the structural and thermodynamic constraints that limit long-term cycling in aqueous media. Mechanistic indicators of reversibility, including peak separation, current ratios and heterogeneous electron-transfer rate constants, are linked to mediator architecture, coordination chemistry and immobilisation environment. By integrating molecular electrochemistry with applied sensor engineering, this review provides a mechanistically grounded basis for selecting or designing redox mediators that sustain efficient electron transfer, minimal fouling and calibration stability across diverse sensing platforms.

Keywords: redox mediators; reversibility; electron transfer kinetics; electrochemical biosensors; organometallic and inorganic complexes

Check for updates

Academic Editor: Antonino Gulino

Received: 12 December 2025
Revised: 23 December 2025
Accepted: 24 December 2025
Published: 26 December 2025

Copyright: © 2025 by the author. Licensee MDPI, Basel, Switzerland. This article is an open access article distributed under the terms and conditions of the Creative Commons Attribution (CC BY) license.

1. Introduction

Electrochemical biosensors convert biochemical recognition events into electrical signals, with electron transfer (ET) between a redox-active biocatalyst and an electrode forming the key transduction step [1]. For many oxidoreductases, the catalytic cofactors (e.g., flavin adenine dinucleotide (FAD), heme or copper centres) are embedded within the protein matrix, hindering direct ET [2]. To overcome this kinetic barrier, redox mediators, such as small organic molecules, organometallic species, coordination complexes, polymers or nanostructured hybrids, are employed to shuttle electrons between the enzyme and the electrode surface [3,4].

A defining characteristic of an efficient mediator is its reversible redox behaviour [5]. In this review, 'reversibility' refers to the mediator's ability to undergo repeated oxidation and reduction while maintaining both chemical integrity and electrochemical performance.

Chemical recoverability of the redox states is therefore the central criterion, supported by electrochemical indicators such as peak separation (ΔE_p), current ratios (i_{pa}/i_{pc}) and the heterogeneous electron-transfer rate constant (k°). High reversibility supports stable current output, reduced electrode fouling, predictable ET kinetics and reproducible analytical performance [4,6]. In contrast, irreversible or quasi-reversible mediators often induce potential drift and decreased activity, and require frequent recalibration [1].

Historically, mediator development has shaped biosensor evolution. First-generation sensors relied on molecular oxygen as the terminal electron acceptor but were constrained by poor solubility and the irreversibility of oxygen reduction [4]. Second-generation systems introduced synthetic mediators such as ferrocene (Fc), quinones and phenazines, enabling controlled outer- or inner-sphere ET and tuneable redox potentials [7–9]. While third-generation devices aim for mediator-free direct ET, practical biosensing continues to depend heavily on mediated approaches due to their engineered stability, potential control and reproducibility [3,6].

At the molecular level, reversibility is strongly influenced by the coordination environment, ligand field, spin state and electron-transfer mechanism, particularly for metal-based mediators such as Fc derivatives, ruthenium and osmium polypyridyl complexes, cobalt macrocycles and Prussian Blue (PB) analogues [7–11]. These systems often support robust, outer-sphere ET pathways that maintain chemical recoverability of both redox states and define the upper limits of reversible cycling in aqueous media. Their behaviour contrasts with that of many organic mediators, such as quinones and phenazines, in which proton-coupled ET (PCET), hydration, semiquinone formation and polymerisation frequently lead to loss of reversibility under operational conditions [7–9,12].

The scope of this review is to examine inorganic, organometallic and organic mediators through the lens of reversibility as a mechanistic design principle, with emphasis on literature published since 2010, when stability and mechanistic understanding became central criteria. Foundational earlier studies are included where they provide essential mechanistic context. Organic mediators considered here include quinones and catechols, phenazines, viologens, indophenols, aminophenols, azines, phenothiazines and phenoxazines. The inorganic and organometallic families surveyed encompass Fc derivatives, ruthenium and osmium polypyridyl complexes, iron and cobalt coordination compounds and PB analogues. Hybrid systems, including mediator-enzyme co-immobilised assemblies, are also discussed, as they inform the mechanistic analysis. Cyclic voltammetry (CV) is used throughout as the primary probe of electron-transfer kinetics and reversibility.

By centring the analysis on reversibility, this review establishes a unifying framework for comparing mediator classes and guiding the design of next-generation systems. The discussion links molecular structure, coordination chemistry and electron-transfer behaviour to measurable electrochemical performance, identifying how reversible mediators contribute to stability and reproducibility in biosensors.

Although numerous reviews have summarised the synthesis and use of specific mediator classes, such as quinones and Fc derivatives [9,12–17], these typically emphasise material development or analytical performance rather than the mechanistic determinants of electrochemical reversibility. In contrast, this review bridges inorganic, organic and physical electrochemistry with applied biosensor engineering. By correlating CV parameters with long-term stability, fouling tolerance and calibration drift, it provides a mechanistically grounded framework for selecting or engineering mediators suited to complex sample matrices.

Throughout this review, electrochemical potentials are reported versus Ag/AgCl, 3 M NaCl, wherever possible. When the original literature did not specify the chloride concentration of the Ag/AgCl reference electrode, or when pseudo-reference electrodes

were employed, the potentials are reported as originally stated and clearly indicated in the corresponding table footnotes. No further conversion was applied in these cases to avoid introducing uncertainty or artificial offsets.

Accordingly, this review is not intended as a comprehensive catalogue of individual ligand families or coordination motifs, but rather as a cross-class analysis of reversibility as a functional design constraint in biosensing applications.

Defining Reversibility in Redox Mediators

In electrochemical terms, reversibility denotes a redox process in which the forward and reverse electron-transfer reactions are sufficiently fast that equilibrium between oxidised and reduced forms is maintained during potential cycling [18]. Operationally, this is assessed by CV, which examines the ΔE_p and the i_{pa}/i_{pc} ratio. A mediator exhibiting ΔE_p~59 mV $\times$ n^{-1} at 25 °C and i_{pa}/i_{pc}~1 is considered electrochemically reversible under diffusion control [18].

The Matsuda–Ayabe criteria provide a quantitative framework for distinguishing between electrochemically reversible, quasi-reversible, and irreversible systems. This dimensionless kinetic parameter Λ is defined in Equation (1),

$$\Lambda = \frac{k^0}{\sqrt{\frac{\pi n F v D}{RT}}} \quad (1)$$

where D is the diffusion coefficient (assuming $D_{ox} \approx D_{red}$), v the scan rate, n the number of electrons, R the gas constant, and T the temperature in Kelvin [19,20]. Systems with $\Lambda > 15$ are electrochemically reversible, with $15 > \Lambda > 10^{-3}$ are quasi-reversible, and with $\Lambda < 10^{-3}$ are irreversible [21].

From the perspective of biosensor operation, reversibility must also encompass chemical sustainability, since mediators experience repeated cycling under non-ideal conditions. Practical reversibility, therefore, integrates two complementary aspects [18]:

1. Electrochemical reversibility: rapid interfacial ET yielding near-Nernstian voltammetry, defined by small ΔE_p and high k°.
2. Chemical reversibility: structural and chemical integrity of the mediator during continuous redox cycling without decomposition, dimerisation, ligand loss, or adsorption.

Additionally, mediator performance is governed by [18,22] the following:

(a) Physical retention: mediator leaching from the electrode or matrix should be minimal to maintain a consistent signal amplitude.
(b) Biocompatibility: reversible mediators should not inactivate the enzyme or generate reactive intermediates that compromise electrode integrity.
(c) Environmental robustness: redox reversibility should persist across realistic variations in pH, ionic strength, temperature and potential cycling frequency.

Quantitatively, Laviron and Marcus–Hush models are frequently applied to extract k° and transfer coefficients (α), which together provide a kinetic measure of reversibility [18,19,21]. Using Λ, fully reversible behaviour ($\Lambda > 15$) typically requires k°~0.05–0.17 cm s^{-1} for v = 0.01–0.10 V s^{-1} when D~10^{-5} cm^2 s^{-1}. Values around k°~1.0 $\times$ 10^{-2} cm s^{-1} correspond to quasi-reversible regimes at these scan rates (v). Complementary methods, such as electrochemical impedance spectroscopy and chronoamperometry, assess mediator stability and ET efficiency during extended operation [5]. Whereas organic mediators commonly rely on PCET, substituent-controlled frontier orbitals, and significant structural reorganisation, organometallic and coordination-based mediators derive their behaviour from rigid ligand fields and metal-centred redox manifolds that yield low reorganisation energies and highly predictable ET responses.

In this review, reversibility therefore denotes the combined electrochemical and chemical sustainability of the mediator. Framing the discussion around this dual definition enables mechanistic comparison between organic, inorganic and hybrid systems, clarifying how redox reversibility underpins the long-term reliability of an electrochemical biosensor. While both organic and inorganic mediators are widely employed, the uniquely tuneable and structurally rigid redox centres found in organometallic and coordination compounds underpin many of the most advanced biosensing architectures, motivating renewed interest in their systematic design.

2. Organometallic and Inorganic Mediators

Organometallic and inorganic mediators occupy a central position within the redox-mediator landscape because their electrochemical behaviour is governed by metal-ligand orbital interactions, ligand-field architecture, and predictable d-orbital manifolds, rather than by the proton-coupled or π-framework dynamics that dominate most organic dyes. Whereas reversibility in viologens, quinones, phenazines and phenoxazines is determined by substituent-driven modulation of frontier orbitals, proton-coupled equilibria and large reorganisation energies, metal-centred systems achieve near-ideal outer-sphere ET by imposing rigid coordination geometries that minimise structural distortion during redox cycling [18,23]. These features give rise to modular and tuneable redox couples across a broad mid-to-positive potential region, complementing the deeper negative potentials typically accessible to quinones and viologens and thereby expanding the electrochemical window available for biosensor design.

Their relevance becomes especially clear in applications where (*i*) precise potential matching to enzyme cofactors is required; (*ii*) reversible ET must be preserved under polymer or matrix confinement; (*iii*) operation must occur at potentials incompatible with the chemical stability of quinones or dyes; or (*iv*) oxygen interference must be circumvented.

Ferrocene derivatives, osmium polypyridyl complexes, ruthenium bipyridyl systems, cobalt macrocycles and related metal-ligand frameworks collectively address these demands. Their formal potentials, $E^{\circ\prime}$, can be tuned over more than 1 V by modifying metal identity, ligand donor strength, axial coordination, or the surrounding microenvironment, enabling mediator design for FAD-, NAD-(nicotinamide adenine dinucleotide), PQQ-(pyrroloquinoline quinone), haem- and copper-dependent enzymes [23].

Mechanistically, most organometallic and inorganic mediators operate through outer-sphere ET, avoiding changes in coordination geometry, ligand protonation states or metal-ligand bond order during redox cycling. This sharply contrasts with organic proton-coupled electron-transfer systems, where protonation, tautomerisation or semiquinone formation frequently modulate voltammetric signatures. As a result, polypyridyl complexes and metallocenes typically exhibit low reorganisation energies, fast heterogeneous electron-transfer kinetics and stable Nernstian cycling even under repeated operation or challenging electrochemical conditions [18,23]. When incorporated into redox polymers or covalently tethered architectures, these complexes retain their electrochemical identity while supporting efficient electron hopping or through-bond transport, which is difficult to achieve with most small organic mediators.

Nevertheless, they are not universally superior. Their design space is constrained by aqueous stability, ligand-exchange susceptibility, toxicity considerations and synthetic cost, attributes that must be weighed carefully against their tunability and reversibility. Osmium redox polymers provide unmatched oxygen-independent wiring of oxidoreductases; Fc offers exceptional modularity; and cobalt complexes contribute ligand-controlled inner-sphere pathways and catalytic versatility within a mid-potential region where many organic mediators suffer from chemical instability. Consequently, organometallic and inorganic

mediators play a structurally and mechanistically dominant role in expanding the accessible electrochemical design space, offering tunability and stability profiles that complement, and often exceed, those of purely organic mediator classes [23–25].

This conceptual framework motivates the following subsections, which examine Fc and osmium-, iron-, ruthenium-, and cobalt-based mediators, emphasising their mechanistic behaviour, potential tunability, immobilisation chemistry, and demonstrated biosensing performance.

2.1. Ferrocene

Ferrocene occupies a central position in organometallic mediator design because its Fe^{2+}/Fe^{3+} oxidation is a prototypical outer-sphere electron-transfer process with exceptionally low reorganisation energy. The metal centre undergoes a clean, reversible one-electron transformation without bond-breaking, ligand rearrangement, or proton transfer, and its framework remains essentially invariant between redox states [26]. This absence of coupled chemical steps distinguishes Fc/ferrocenium (Fc^+) from organic mediators that engage in PCET, tautomerisation or radical-radical processes (see below). In aqueous systems, water-compatible ferrocenyl derivatives (Figure 1) typically exhibit $E^{\circ\prime}$ between 0.25 and 0.45 V vs. Ag/AgCl, 3 M NaCl, with the exact value governed by substituent electronics and the local microenvironment [27,28]. The rigidity of the η^5-cyclopentadienyl coordination sphere and minimal geometric change upon oxidation account for Fc's highly Nernstian behaviour and its long-standing role as a benchmark reversible mediator in both solution-phase and immobilised biosensing platforms [27,28].

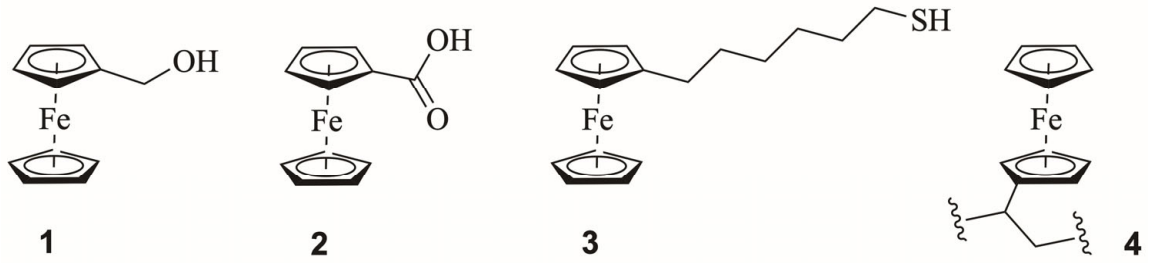


Figure 1. Representative ferrocene mediators spanning solution-phase derivatives, including ferrocenemethanol (**1**) and ferrocenecarboxylic acid (**2**); the SAM-forming unit 6-ferrocenylhexanethiol (**3**) as a model surface-bound architecture; and poly(vinylferrocene) (**4**) as a prototypical polymer-confined redox system.

Across aqueous, buffered and polymer-confined environments relevant to biosensors, the Fc/Fc^+ couple retains the hallmarks of a fully reversible outer-sphere redox process. In solution, Fc derivatives consistently exhibit Nernstian peak separations of ca. 59–60 mV for a reversible $1e^-$ process [18], with k° typically in the 10^{-2}–10^{-1} cm s^{-1} range at metal and carbon electrodes [29], placing Fc firmly in the reversible regime under diffusion-controlled conditions, while deviations observed in confined or viscous systems reflect transport and architectural limitations rather than intrinsic ET kinetics. Surface-confined Fc monolayers follow the Chidsey exponential distance-decay relationship, giving $k^\circ \sim 10^2$–10^3 s^{-1} for short alkyl chains [30], while Fc-based redox polymers display broadened yet symmetric voltammetry where the apparent ET rate is governed by polymer segmental mobility rather than intrinsic Fc kinetics [31–33]. Collectively, these quantitative metrics confirm that Fc exhibits intrinsically reversible outer-sphere ET across solution, SAM, and polymer environments, and that any quasi-reversible behaviour observed in biosensors reflects immobilisation geometry, polymer dynamics, or local microenvironmental constraints rather than limitations of the Fc/Fc^+ couple itself.

Because neutral Fc is essentially insoluble in water, biosensor development has relied on derivatised Fc species bearing polar or ionisable groups (e.g., **1**, **2**, sulfonated or quaternary-ammonium Fc) or on Fc-functionalised polymers (Figure 1), in which pendant ferrocene units remain electrochemically addressable despite being immobilised within a hydrated polymer matrix. Substituent modification at the cyclopentadienyl rings allows redox potential, solubility, hydrophilicity and adsorption behaviour to be tuned, although the accessible range depends strongly on the medium. In aqueous electrolytes, water-compatible ferrocenyl derivatives typically vary within a comparatively narrow ca. 0.2 V window. In contrast, in mixed or non-aqueous solvents, the Fc/Fc^+ couple can be shifted by several hundred millivolts without compromising reversibility [34]. These functionalisation sites enable Fc to serve as both a mediator and a local reporter, particularly in affinity sensors, where it is anchored to crown ethers, calixarenes or supramolecular hosts. Binding-induced dielectric, steric or π-interaction changes then modulate its voltammetric behaviour [34].

In immobilised architectures, Fc exhibits behaviours distinct from those of small organic mediators because ET becomes sensitive not only to the intrinsic ET rate constant but also to mediator accessibility, polymer dynamics and hydration state. Ferrocene-terminated SAMs on a gold support exhibit fast, reversible ET when the alkyl tether is short, as in **3**, and when packing is dilute. In contrast, densely packed monolayers or deeply buried ferrocenyl units show markedly slower electron-transfer kinetics [34,35]. Similar constraints arise in chitosan, sol-gel and siloxane matrices: ET rates and apparent reversibility depend strongly on polymer segmental motion, water content and the spatial dispersion of ferrocenyl moieties [14,28]. These observations emphasise that Fc's ideal outer-sphere behaviour is preserved only when the immobilisation geometry avoids insulating the metal centre and ensures efficient mediator-electrode communication.

Fc-based redox polymers, poly(vinylferrocene) (**4**), Fc-grafted polysiloxanes, ferrocenyl poly(ethyleneimine) and other Fc-functional networks extend these principles by enabling multistep electron-hopping pathways along polymer chains. Such architectures support mediator densities and apparent ET rates far exceeding those attainable with small molecules, effectively wiring oxidoreductases that are otherwise electronically insulated [27,28]. Polymer rigidity, hydration and the dielectric profile of the microenvironment govern hopping distance and stability, with well-optimised films displaying prolonged cycling, low drift and compatibility with physiological ionic strengths. These Fc-based redox polymers therefore bridge the gap between classical small-molecule mediators and the more strongly ligand-tuned osmium redox polymers, offering a complementary design space at intermediate potentials.

Ferrocene's limitations arise from the same features that make it attractive. Classical Fc is hydrophobic and poorly soluble in water, necessitating derivatisation or incorporation into polymeric or hybrid matrices. Although Fc^+ is generally stable under physiological conditions, it becomes vulnerable to nucleophilic attack in strongly alkaline media. For wiring high-potential oxidases, challenges typically stem not from the intrinsic Fc/Fc^+ potential, which can be shifted through electron-withdrawing or electron-donating substituents and which spans positive, neutral and negative water-soluble derivatives, but from electrostatic and geometric factors: cationic Fc forms may be repelled by positively charged enzyme channels, and the purely outer-sphere nature of Fc can limit ET at buried or sterically gated active sites. Hydrophobic Fc units may also interact weakly with carbon surfaces, sharpening or distorting voltammetric profiles depending on surface preparation. These limitations are mitigated through Fc-modified chitosan, polysiloxanes, carbon nanotube (CNT)-polymer composites and water-soluble Fc redox polymers, which improve hydrophilicity, mediator dispersion and chemical robustness [14]. Despite these considera-

tions, the combination of reversible outer-sphere ET, modular derivatisation, predictable potential tuning and compatibility with both solution-phase and immobilised architectures establishes Fc as a cornerstone organometallic mediator and a natural reference point for the more strongly ligand-tuned osmium, ruthenium and cobalt complexes discussed below.

2.2. Iron-Based Mediators: Ferricyanide, Ferrocyanide and Prussian Blue

The ferrocyanide/ferricyanide, $[Fe(CN)_6]^{4-}/[Fe(CN)_6]^{3-}$, couple (Equation (2)) remains one of the most widely used inorganic mediators in aqueous electrochemistry due to its textbook outer-sphere Fe^{2+}/Fe^{3+} ET and well-defined redox thermodynamics. In a neutral buffer, the formal potential typically lies between 0.22 and 0.24 V vs. Ag/AgCl, and on polished glassy carbon electrodes, the couple exhibits the characteristic diffusion-controlled currents and well-defined peak shapes that underpin its historical role as a benchmarking redox probe [36,37]. In practical biosensor substrates, however, the behaviour becomes highly substrate-dependent. Screen-printed and composite carbon electrodes, which incorporate binders, surface oxides and microstructured domains, often display broadened voltammograms and altered kinetics due to restricted ion mobility, local adsorption and heterogeneous microenvironments [38,39]. On gold, the mechanistic picture changes fundamentally: $[Fe(CN)_6]^{3-}$ rapidly chemisorbs, forming surface-bound Au-CN intermediates (commonly described as Au-CN-Fe linkages) that restructure the double layer and inhibit classical outer-sphere ET. At the same time, $[Fe(CN)_6]^{4-}$ participates in further adlayer growth once the surface is modified [40,41]. These strong substrate effects create significant challenges when either $[Fe(CN)_6]^{4-}$ or $[Fe(CN)_6]^{3-}$ is used as a mediator, or when the couple is stored directly on metal electrodes in biosensing formats, where electrode pretreatment, microstructure and storage conditions strongly dictate electrochemical performance.

$$[Fe(CN)_6]^{4-} \longrightarrow [Fe(CN)_6]^{3-} + e^- \quad (2)$$

Across these substrates, the intrinsic reversibility of the $[Fe(CN)_6]^{4-}/[Fe(CN)_6]^{3-}$ couple varies dramatically. On polished glassy carbon and other low-defect carbons, ΔE_p values of 60–70 mV at low scan rates and $i_{pa}/i_{pc} \sim 1$ and $v^{1/2}$-dependent peak currents, together with diffusion coefficients near 10^{-6} cm^2 s^{-1} and k° values in the 10^{-2}–10^{-1} cm s^{-1} range, are all consistent with rapid, outer-sphere electron transfer [36,37]. Under these conditions, Matsuda–Ayabe analysis (Equation (1)) places the $[Fe(CN)_6]^{4-}/[Fe(CN)_6]^{3-}$ couple in the reversible regime across typical biosensor scan rates, with only the lower end of the k° range approaching quasi-reversible behaviour at elevated scan rates where uncompensated resistance becomes significant. In contrast, screen-printed carbons typically exhibit ΔE_p values broadened to 150–300 mV at 0.05–0.1 V s^{-1}, diminished peak symmetry, and breakdown of $v^{1/2}$ scaling, indicating quasi-reversible kinetics governed by surface chemistry and microstructured electrolyte domains [38]. On gold, chemisorption-driven inner-sphere behaviour progressively develops, ultimately suppressing classical reversibility and yielding slow, surface-confined electron-transfer signatures [40,41]. Although short exposures may transiently display near-Nernstian behaviour, the $[Fe(CN)_6]^{4-}/[Fe(CN)_6]^{3-}$ couple rapidly loses outer-sphere character as adsorption proceeds. Thus, while intrinsically reversible at well-prepared carbon electrodes, its operational reversibility in biosensors is often severely compromised by substrate interactions, microstructure and adsorptive processes.

In solution-phase assays, $[Fe(CN)_6]^{3-}$ can behave as a competent mediator for oxidases whose reduced cofactors lie well above 0.2 V, including glucose and lactate oxidases. Nevertheless, it is highly susceptible to parasitic chemistry: $[Fe(CN)_6]^{3-}$ oxidises NADH non-selectively, competes with O_2 for reduced flavins, and undergoes slow photodecomposition that releases free cyanide under illumination [36,37]. The $[Fe(CN)_6]^{4-}$ product is also prone to reoxidation by dissolved oxygen, distorting calibrations in low-current

biosensors. In alkaline media, hydroxide competes with cyanide for coordination, destabilising Fe-CN linkages and generating $Fe(OH)_x$ or soluble hexacyanoferrate fragments, a pathway well documented for the chemical degradation of Prussian Blue films [24,42]. These features sharply constrain its use in modern mediator-based biosensing, where stability, reversibility and compatibility with polymer matrices are essential. The behaviour contrasts strongly with Fc derivatives, whose outer-sphere ET and chemical inertness make them more predictable mediators over long operational times.

Where $[Fe(CN)_6]^{4-}/[Fe(CN)_6]^{3-}$ represents a molecular outer-sphere probe, PB introduces a solid-state mixed-valence framework with fundamentally different constraints on reversibility.

Prussian Blue consists of an extended Fe^{3+}-NC-Fe^{2+} mixed-valence lattice capable of reversible solid-state transitions between PB, Prussian White (PW) and Prussian Green (PG). Its electrodeposition proceeds through redox-driven assembly of intact hexacyanoferrate units rather than cyanide loss. Under anodic polarisation, ferrocyanide is first oxidised to ferricyanide at the electrode surface (Equation (2)), which establishes the oxidising conditions required for PB nucleation [24,43]. The ferricyanide produced in situ then coordinates Fe^{2+}, generated chemically or electrochemically from Fe^{3+}, to yield the canonical PB structural unit (Equation (3)),

$$Fe^{2+} + [Fe(CN)_6]^{3-} \longrightarrow Fe^{III}[Fe^{II}(CN)_6] \quad (3)$$

where the cyanide ligands remain bound to Fe^{2+} and adopt μ-CN bridging geometry, binding Fe^{3+} through the nitrogen terminus to generate the extended PB lattice [24,43]. Charge-balancing cations are incorporated to form the hydrated solid (Equation (4)),

$$Fe^{III}[Fe^{II}(CN)_6] + x\,K^+ \longrightarrow K_xFe^{III}[Fe^{II}(CN)_6] \cdot nH_2O \quad (4)$$

and when these elementary steps are combined, the overall electrodeposition from an $Fe^{3+}/Fe(CN)_6{}^{4-}$ bath can be summarised by Equation (5) (formal net reaction):

$$Fe^{3+} + [Fe(CN)_6]^{4-} \xrightarrow{electrodeposition} Fe^{III}[Fe^{II}(CN)_6](s) \quad (5)$$

provided the growth medium remains sufficiently acidic to prevent Fe^{3+} hydrolysis and cyanide displacement [43]. During operation, PB undergoes reversible reduction to PW (Equation (6)) and oxidation to PG (Equation (7)):

$$Fe^{III}[Fe^{II}(CN)_6] + K^+ + e^- \longrightarrow KFe^{II}[Fe^{II}(CN)_6] \quad (6)$$

$$Fe^{III}[Fe^{II}(CN)_6] \longrightarrow Fe^{III}[Fe^{III}(CN)_6] + e^- \quad (7)$$

The E°′ for the PB/PW couple typically lies around 0.10 to 0.20 V vs. Ag/AgCl, enabling low-potential reduction of hydrogen peroxide through an EC′ process (electrochemical reduction of PB followed by catalytic chemical regeneration by H_2O_2) that gives PB its role as an "artificial peroxidase." Operating at such low potentials suppresses electrochemical interferents, making PB valuable in oxidase-based sensors where H_2O_2 is the terminal reporter [42].

Prussian Blue films can exhibit near-ideal PB/PW reversibility only under tightly controlled structural and electrolyte conditions. Thin, well-crystallised PB films electrodeposited in acidic KCl display sharp PB/PW transitions with ΔE_p as low as 15–30 mV at 0.01–0.02 V s^{-1} and symmetric peak currents whose scan-rate dependence lies between surface-confined ($i \propto v$) and diffusion-controlled ($i \propto v^{1/2}$) behaviour, reflecting rapid mixed-valence conduction and efficient lattice utilisation [24,44]. Under such optimised conditions,

apparent rate constants for PB/PW conversion and for the associated EC′ reduction of H_2O_2 can exceed 10^{-2} cm s^{-1}, consistent with PB's behaviour as an artificial peroxidase [43]. As PB films become thicker, less hydrated, or K^+-deficient, ΔE_p broadens to 80–150 mV, scan-rate dependence increases, and accessible charge decays due to finite ion mobility and formation of inactive domains, a pattern frequently reported for PB-nanotube and PB-oxide composites [38,45]. Prussian Blue is intrinsically pH-sensitive: above pH~7, the Fe^{2+}/Fe^{3+}-CN framework undergoes hydroxide-driven lattice dissolution, forming soluble ferricyanide species, while prolonged cycling promotes K^+/H^+ redistribution, Fe-vacancy accumulation and partial oxidation to PG [42,46]. Long-term storage, particularly in the dry state, often yields PB analogues with altered stoichiometry, shifted potentials, and diminished reversibility [24,44]. Prussian Blue films further exhibit variable adhesion to gold, carbon and metal-oxide substrates, and their mechanistic performance is strongly dependent on hydration state, thickness and K^+ availability [41,43].

Taken together, ferricyanide, ferrocyanide and Prussian Blue represent the oldest and most widely used inorganic mediator systems. Yet, they lack the structural and electrochemical robustness of modern metallopolymer mediators such as Fc, Ru- and Os-polypyridyl complexes. Their behaviour deviates significantly from the ideal of chemically reversible, outer-sphere ET: $[Fe(CN)_6]^{4-}$ suffers from adsorptive and ligand-exchange complications, pronounced interaction with gold surfaces and photolability, while Prussian Blue exhibits pH-limited stability, lattice dissolution and slow degradation under repeated cycling. Although both systems retain value in specific low-cost or legacy assay formats, their limitations place strict constraints on their deployment in contemporary biosensing architectures, and they are unsuitable for mediator-enzyme coupling strategies that rely on long-term redox cycling, immobilisation or polymer-based ET enhancement.

2.3. Osmium Complexes and Polymers

Osmium polypyridyl complexes (examples in Figure 2) constitute one of the most tuneable and electrochemically robust mediator families for aqueous biosensing. The Os^{2+}/Os^{3+} couple is a clean outer-sphere process with negligible structural reorganisation. The resulting one-electron redox transition is fully reversible, showing no ligand exchange or proton-coupled rearrangement and retaining Nernstian behaviour in aqueous and polymeric environments [23,37]. The formal potential can be modulated over nearly 0.6 V by simple ligand-field variation, and the experimental values reported in aqueous buffer span from cathodic mixed-ligand complexes such as $[OsCl(im)(dmbpy)_2]^{2+}$ at −0.01 V vs. Ag/AgCl to strongly anodic tris-bipyridine species such as $[Os(bpy)_3]^{2+}$ at 0.61 V [47]. Parallel studies on substituted tris(4,4′-substituted bipyridine) complexes confirm that electron-donating 4-alkoxy and 4-dialkylamino substituents depress the redox potential of the complex, with potentials reaching −0.33 V for $[Os(dmabpy)_3]^{2+}$ [48]. In contrast, unsubstituted or π-accepting ligands push E°′ towards the positive potential limit [47,48]. These ligand-governed shifts directly correspond to the values summarised in Table 1, which consolidates aqueous potentials for both discrete complexes and polymer-bound Os species.

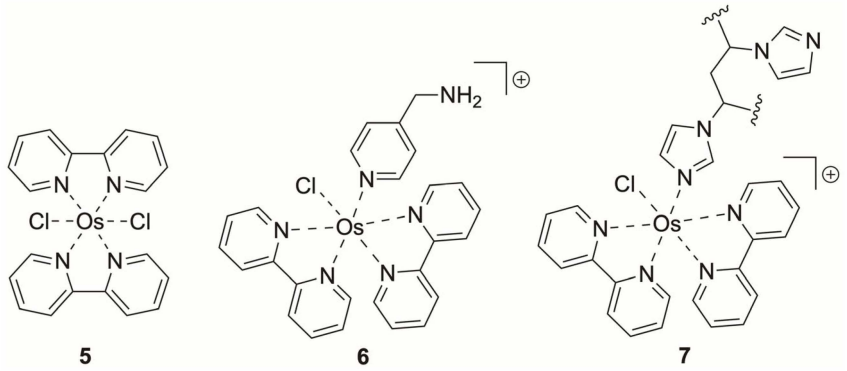


Figure 2. Representative osmium redox mediators used in enzymatic biosensing: (**5**) parent bis(bipyridyl)Os(II) complex, forming the basis of most osmium polypyridyl mediator families, (**6**) tetherable Os(II) complex coordinated through the pyridine nitrogen, with a pendant amine for covalent attachment, (**7**) polymer repeat unit showing Os(II) coordination to the imidazole nitrogen of poly(Vim).

Table 1. Formal potentials of representative osmium complexes and redox polymers in aqueous media.

Mediator	E°′ (V) *	Key Applications	Ref.
$[Os(bpy)_3]^{2+}$	0.61	Model ET standard; benchmark for ligand effects	
$[Os(dmbpy)_3]^{2+}$	0.43	Prototype low-bias mediator; guidance for polymer design	
$[Os(bpy)_2(im)_2]^{2+}$	0.29	Mimics histidyl coordination; haem-protein wiring models	[47]
$[Os(dmbpy)_2(im)_2]^{2+}$	0.15	Low-overpotential ET to FAD/PQQ centres	
$[Os(bpy)_2Cl(im)]^{+}$	0.11	Testbed for axial-ligand tuning, chloride lability	
$[Os(bpy)_2ClpyCOOH]^{+}$	0.17	HRP mediator for low-bias flow immunoassay	[49]
Poly(Vim)-$[Os(bpy)_2Cl]$	−0.25	Early GOx redox hydrogel; Type-II glucose sensors	
Poly(Vim)-$[Os(dmbpy)_2Cl]$	−0.10	GOx anodes and laccase cathodes in glucose–O_2 fuel cells	
Poly(Vim)-$[Os(dmObpy)_2Cl]$	−0.07	High-power GOx anodes at near-zero bias	
Poly(Vim)-$[Os(dabpy)_2Cl]$	−0.15	Pseudo-physiological GOx anodes; PBS at pH 7.4	[2]
Poly(Vpy)-$[Os(bpy)_2Cl]^{+}$	0.35	PQQ-GDH/BOx fuel cells; cathodic mediators	
Poly(Vim)-$[Os(phen)_2(im)_2]^{2+}$	0.49	Laccase cathodes in neutral buffer; O_2 reduction	
Poly(Vim)-$[Os(bpy)_2Cl]$	0.15	Generic oxidase wiring; PCET-free reference system	
Poly(Vim)-$[Os(bpy)_2O_2]$	0.50	Illustrates detrimental effect of unintended oxo ligation	[50]

* Formal potentials reported in phosphate/MOPS/PBS buffers against Ag/AgCl, 3 M NaCl. Potential values reported vs. alternative reference electrodes were converted using Ag/AgCl, 3 M NaCl; Ag/AgCl, 0.1 M KCl and Ag/AgCl, sat. KCl = −0.034, 0.047, −0.042V vs. SCE, respectively [51,52].

Across both discrete complexes and polymer-bound hydrogels, the Os^{2+}/Os^{3+} couple exhibits one of the most reliably reversible electrochemical behaviours among inorganic mediators. Tris-bipyridyl and mixed-ligand complexes typically display ΔE_p values of 55–70 mV at 0.01–0.02 V s^{-1} with i_{pa}/i_{pc}~1, confirming fast outer-sphere ET and negligible structural reorganisation upon oxidation [47,53]. Analyses of $[Os(bpy)_2Cl(im)]^{+}$ and related species report heterogeneous rate constants k° in the 10^{-2}–10^{-1} cm s^{-1} range, comparable to Fc but with superior ligand stability under cycling [48]. When incorporated into Poly(1-vinylimidazole), poly(Vim) or poly(vinylpyridine), poly(Vpy), hydrogels, the Os centres remain chemically reversible, but the voltammetry broadens due to finite electron-hopping transport: classic poly(Vim)-Os films show ΔE_p~90–120 mV at 0.1 V s^{-1} and apparent diffusion coefficients D~10^{-8}–10^{-6} cm^2 s^{-1}, the upper limit reached in highly hydrated, lightly crosslinked formulations [23,53]. More modern pendant-imidazole and amine-rich architectures further enhance mobility, yielding D values approaching 10^{-6} cm^2 s^{-1} and narrower ΔE_p profiles under matched hydration [54,55]. Importantly, Os^{3+} centres generated during cycling remain ligand-retentive and resist aquation or oxo formation under operational potentials, preserving

chemical reversibility even during hours-long amperometry [37,56]. Deviations from ideal Nernstian behaviour therefore arise primarily from polymer microstructure, such as hydration, crosslinking density, counter-ion transport and local dielectric environment, rather than from instability of the Os^{2+}/Os^{3+} redox couple itself.

Kinetic analyses demonstrate that these thermodynamic adjustments do not compromise the efficiency of mediation. Mixed-ligand complexes operating near 0.0 V, including $[OsCl(im)(dmbpy)_2]^{2+}$, sustain mediation rate constants on the order of 10^5 M^{-1} s^{-1}, exceeding the performance of Fc carboxylates under comparable conditions [47]. Conversely, bipyridines bearing ionisable substituents (e.g., carboxylates or phenolates under alkaline conditions) can exhibit diminished electron-transfer rates due to increased ligand charge and altered interfacial interactions, despite favourable driving force [48], illustrating that long-range electrostatics can govern mediator-enzyme coupling as strongly as formal potential. Spectroelectrochemical studies across both discrete complexes and hydrogels further confirm that Os^{3+} centres do not undergo ligand loss or rearrangement during prolonged cycling, maintaining intact coordination spheres under operational bias [57,58].

For practical biosensing, osmium complexes are almost exclusively used as redox polymers, in which covalent tethering and electron hopping enable long-range wiring of buried redox cofactors. Poly(Vim) and poly(Vpy) architectures dominate this space due to strong N-donor anchoring and favourable hydration properties [25,59]. Early Type-II poly(Vim)-$[Os(bpy)_2Cl]$ hydrogels exhibit $E^{\circ\prime}$ of ca. -0.25 V [2], whereas later pendant-imidazole formulations shift $E^{\circ\prime}$ into the 0.20 to 0.33 V range, better matching oxidase operating windows [2]. Analogous trends extend across substituted bipyridine ligands: poly(Vim)-$[Os(dmbpy)_2Cl]$ and poly(Vim)-$[Os(dmObpy)_2Cl]$ shift the potential to -0.10 V and -0.07 V, respectively, while electron-rich diamino-bipyridine analogues reach -0.15 to -0.11 V, permitting ultra-low-bias operation of FAD-, PQQ- and haem-based oxidases [2]. At the positive limit, phenanthroline complexes such as poly(Vim)-$[Os(im)_2(phen)_2]^{2+}$ reach 0.49 V and are suited for laccase cathodes and other high-potential systems [2].

In their crosslinked polymer form, these poly(Vim) and poly(Vpy)-bound osmium complexes behave as hydrated redox hydrogels, in which electron transport proceeds by site-to-site hopping with apparent diffusion coefficients in the 10^{-7}–10^{-6} cm^2 s^{-1} range, enabling efficient wiring of cofactors positioned tens of nanometres from the electrode surface [50,53]. Film mobility is strongly dependent on hydration and crosslinking; excessive rigidity electronically isolates osmium centres and diminishes current density despite favourable redox thermodynamics [25,59]. The polymer microenvironment also influences selectivity: oxidase electrodes employing Os-poly(Vim) exhibit suppressed oxygen interference because the mediator potentials are below the O_2/OH^- couple [60].

Stability considerations further distinguish osmium from other transition-metal mediators. Octahedral $[Os(bpy)_2Cl(L)]^+$ complexes, where the sixth ligand L is typically water, chloride or an imidazole donor in polymer-bound systems, exhibit exceptional resistance to ligand exchange. Chloride-containing species are notably resistant to photoaquation, in contrast to the chloride-labile Ru analogues that undergo photochemical drift in their redox potential [23]. Nevertheless, care is required during synthesis and storage, as inadvertent oxo formation can generate species such as poly(Vim)-$[Os(bpy)_2O_2]$, which shifts the redox potential to 0.50 V and disrupts mediator-enzyme matching [50]. Advances in polymer design, particularly pendant amine and imidazole-rich frameworks, have improved immobilisation strength and reduced leaching [56,61], though crosslink over-densification remains a limiting factor for high-rate electron transport [59].

Collectively, these mechanistic, structural and electrochemical characteristics establish osmium polypyridyl complexes as among the most effective inorganic mediator classes for coupling enzymes to electrodes. Their broad, synthetically adjustable potential window, ro-

bust outer-sphere behaviour, resistance to ligand loss and compatibility with hopping-based redox polymers make Os^{2+}/Os^{3+} systems the benchmark for low-overpotential enzymatic sensing across glucose, lactate, alcohol, choline and PQQ-dependent platforms [2,50,60]. However, these advantages come with substantial practical constraints. Osmium is considerably more expensive than iron-, cobalt- or ruthenium-based alternatives, and the high cost of Os precursors, combined with the need for covalent immobilisation and polymer crosslinking to prevent leaching, limits its suitability for high-volume disposable devices. Even modest Os loadings significantly affect total reagent cost, making widespread deployment in commercial strips or point-of-care cartridges economically challenging despite excellent analytical performance.

2.4. Ruthenium Complex Mediators

Ruthenium polypyridyl and amine complexes constitute an important mediator class whose geometry and outer-sphere kinetics resemble osmium systems, yet their Ru^{2+}/Ru^{3+} couples more frequently fall at mid- to high-positive potentials in biologically relevant media. In aqueous buffer, the formal potential spans approximately from −0.16 to 0.45 V vs. Ag/AgCl, 3 M NaCl, governed by ligand-field strength, coordination environment and ionic medium [45,62–66]. Amine-rich complexes such as $[Ru(NH_3)_6]^{3+}$ and several polymer-bound Ru centres lie at the lower end of this range (Table 2), whereas tris-bipyridine, phenanthroline and cyclometalated species, including $[Ru(phpy)(bpy)_2]^+$ and $[Ru(topy)(bpy)_2]^+$, appear near or above 0.20 V [62,63,65,67]. Electron-donating substituents depress the potential, as in $[Ru(phpy)(dmbpy)_2]^+$, while electron-withdrawing or strongly coordinating ligands such as carboxylates or sulfonates stabilise Ru^{3+} and shift E°′ positively [62,65,67]. These tuneable trends yield a potential window that overlaps extensively with osmium systems, though Ru mediators used in enzyme wiring typically occupy a somewhat narrower mid-positive region within this range.

Table 2. Representative ruthenium mediator complexes assessed in aqueous or buffered media.

Mediator Complex	E°′ (V) *	Key Biosensing Applications	Ref.
$[Ru(NH_3)_6]^{3+}$	−0.16	DNA and aptamer-based sensors; nucleic acid redox tagging; charge compensation and redox cycling in polyelectrolyte or DNA films	[68]
$[Ru(phpy)(bpy)_2]^+$	0.25	HRP-mediated oxidation of catechol and other peroxidase substrates; evaluation of rate constants for HRP isoenzymes	[62]
$[Ru(phpy)(dmbpy)_2]^+$	0.15	Fast redox mediator for plant peroxidases with high apparent second order rate constants for H_2O_2 driven oxidation	
$[Ru(topy)(bpy)_2]^+$	0.20	Peroxidase catalysis with efficient oxidation of catechol at low mediator loading; comparison of anionic and cationic peroxidases	
$[Ru(phendione)_3]^{2+}$	−0.13	Redox mediator for lactate and malate dehydrogenases through NAD^+/NADH cycling	[63]
$[(bpy)_2(NH_3)Ru^{III}(\mu\text{-}O)Ru^{III}(NH_3)(bpy)_2]^{4+}$	0.10	Glucose biosensor where the oxo-bridged Ru complex mediates ET between immobilised GOx and glassy carbon at low bias	[69]
Poly(Vpyr-co-aa)-$[Ru(NH_3)_5]$	−0.14	GOx wired to Ru complex on glassy carbon; low applied potential eliminates interference from ascorbic acid, dopamine and uric acid in glucose sensing	[64]

* Formal potentials reported vs. Ag/AgCl, 3 M NaCl. Potential values reported vs. alternative reference electrodes were converted using Ag/AgCl, 3 M NaCl; Ag/AgCl, 0.1 M KCl and Ag/AgCl, sat. KCl = −0.034, 0.047, −0.042 V vs. SCE, respectively [51,52].

Across both discrete complexes and polymer-bound architectures, ruthenium mediators display a wider spectrum of reversibility than their osmium analogues. Classical outer-sphere complexes such as $[Ru(NH_3)_6]^{3+}$ exhibit near-Nernstian behaviour on carbon, gold and oxide electrodes, with ΔE_p = 55–70 mV at 0.01–0.02 V s^{-1}, i_{pa}/i_{pc}~1, and heterogeneous rate constants k° in the 10^{-2}–10^{-1} cm s^{-1} range, confirming rapid ET with minimal structural reorganisation [63,70,71]. In contrast, most Ru polypyridyl complexes show quasi-reversible Ru^{2+}/Ru^{3+} electrochemistry, with ΔE_p typically 80–120 mV and k° = 10^{-3}–10^{-2} cm s^{-1}, reflecting slower self-exchange kinetics relative to osmium analogues [64,72,73]. Upon immobilisation in redox polymers, including poly(Vpy), poly(Vim), sol–gel matrices and mixed-functional hydrogels, Ru centres remain chemically reversible. Yet, voltammetric profiles broaden due to finite electron hopping and ion-transport limitations, where the ΔE_p values commonly reach 90–150 mV at 0.1 V s^{-1}, with apparent diffusion coefficients D in the 10^{-8}–10^{-6} cm^2 s^{-1} range in hydrated films [62,66,69,71]. These deviations arise primarily from polymer microstructure, hydration and crosslink density rather than from instability of the Ru^{2+}/Ru^{3+} centre, which generally retains its coordination sphere over operational potential windows.

The archetypal mediator $[Ru(NH_3)_6]^{3+}$ avoids the surface sensitivity of the $[Fe(CN)_6]^{4-}$/$[Fe(CN)_6]^{3-}$ couple and displays ideal diffusion-controlled behaviour, supporting a clean outer-sphere mechanism [62,64]. Its high charge drives strong localisation within polyanionic films such as DNA, heparin and carboxylated polymers, making it a widely used charge-reporting probe in nucleic acid sensors where total reductive charge reflects phosphate loading [62,64,66]. The same rapid Ru^{2+}/Ru^{3+} cycling underpins electrografting and metallisation schemes in which Ru^{3+} oxidises surface-bound phenols or anilines, enabling the formation of conductive films under mild aqueous conditions [74,75].

Polypyridyl ruthenium complexes broaden mediator functionality through structural tunability and intrinsic photophysics. $[Ru(bpy)_3]^{2+}$, $[Ru(dmbpy)_3]^{2+}$ and $[RuCl_2(phen)_2]$ typically show formal potentials of 0.35 to 0.45 V versus Ag/AgCl and undergo reversible Ru^{2+}/Ru^{3+} oxidation with modest structural rearrangement [63,65,67,69]. Their stability enables incorporation into redox polymers and hydrogels that support electron-hopping pathways, though lower self-exchange rates reduce hopping efficiency relative to osmium systems [45,69]. Carboxylated bipyridines and iminodiacetate ligands enable covalent polymer attachment, improving immobilisation robustness and expanding compatibility with oxidoreductases such as glucose dehydrogenase (GDH), alcohol dehydrogenase and PQQ-dependent dehydrogenases [65,67]. However, because most ruthenium mediators occupy a narrower and slightly more anodic portion of the potential window than osmium analogues, they cannot access the lowest-bias regimes achievable with Os systems. This restricts their suitability for wiring low-potential cofactors such as $FADH_2$ or reduced haem and increases susceptibility to oxygen reduction and oxidation of endogenous interferents [66,69,73].

Ruthenium complexes also form the basis of major photoelectrochemical and electrochemiluminescent platforms. Tris(bipyridyl) and tris(phenanthroline) derivatives show strong metal-to-ligand charge transfer absorption and long-lived excited states, enabling excitation-driven redox cycling and light emission central to immunoassays, DNA assays and multiplexed biosensing [62,63,76]. Their photodynamics are highly sensitive to polymer hydration, ionic strength and ligand substitution, which jointly tune both excited-state behaviour and the Ru^{2+}/Ru^{3+} potential [63,73,76].

Despite their strengths, ruthenium mediators present several constraints relative to osmium and organic systems. Their positive operating potentials increase oxygen-reduction currents and amplify susceptibility to parasitic oxidation in complex samples [66,69,73]. Many Ru^{2+} polypyridyl complexes undergo photoaquation or ligand loss under illumina-

tion or extended bias, leading to drift in formal potential and diminished mediator loading [45,63,69]. Additionally, ruthenium compounds are costly, and access to polypyridyl derivatives often requires multistep ligand exchange and chromatographic purification, limiting suitability for high-volume disposable sensors [62,63,67]. Although less toxic than osmium analogues, ruthenium species still require strict confinement and minimal leaching in biomedical contexts [45,63]. Collectively, these factors position ruthenium complexes as potent yet specialised mediators, best deployed when their unique outer-sphere kinetics or photochemical properties deliver advantages not achievable with lower-cost mediator classes.

2.5. Cobalt Complex Mediators

Cobalt complexes occupy an intermediate position between classical outer-sphere mediators such as osmium and ruthenium polypyridyls and purely catalytic nanomaterials. Their Co^{2+}/Co^{3+} couples are predominantly inner-sphere in character, often involving axial ligand coordination or substrate binding, and the degree of reversibility depends strongly on ligand structure, pH and immobilisation strategy. In aqueous media, cobalt phthalocyanine (**8**) and porphyrin (**9**) centres (Figure 3) typically display Co^{2+}/Co^{3+} formal potentials between approximately 0.0 and 0.30 V vs. Ag/AgCl, with electron-donating ring substituents shifting the potential in the negative direction and electron-withdrawing or carboxylated groups shifting the potential positively [77–81]. This situates cobalt complexes within the mid- to high-potential region characteristic of aminophenols and indophenols, but at substantially more positive potentials than those of viologens, phenazines or low-potential quinones.

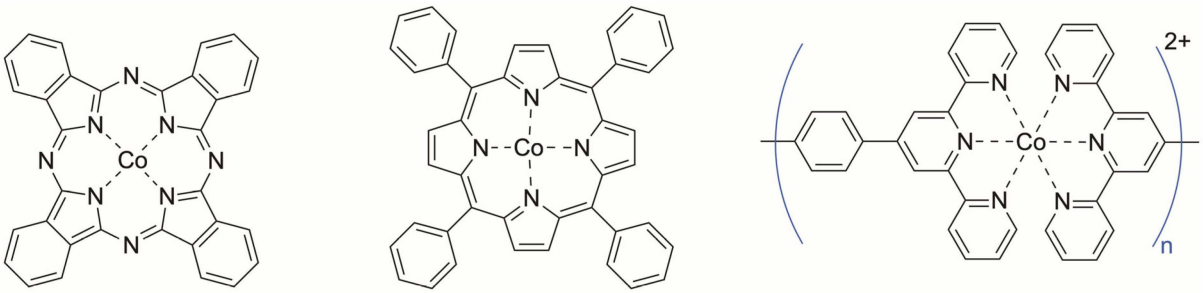


Figure 3. Representative cobalt-based redox mediators used in electrochemical biosensing. (**8**) Cobalt(II) phthalocyanine, (**9**) cobalt(II) tetraphenylporphyrin and (**10**) a generic repeat unit of a cobalt coordination polymer, where the brackets indicate the polymer repeat unit and *n* denotes the degree of polymerisation.

Across both cobalt macrocycles and coordination-polymer systems, the Co^{2+}/Co^{3+} couple rarely approaches the near-Nernstian behaviour observed for classical outer-sphere mediators [77–80,82,83]. Surface-confined cobalt phthalocyanines and porphyrins generally display broad, scan-rate-dependent waves with ΔE_p values well above 100 mV at 0.02–0.1 V s^{-1} and i_{pa}/i_{pc} ratios that deviate from unity as catalytic H_2O_2 turnover overlaps the redox response [77–80,82,83]. Covalent pentamers, cobalt–porphyrin monolayers on gold, and carbon-supported phthalocyanines all exhibit a quasi-reversible Co^{2+}/Co^{3+} wave overlaid by EC′ catalysis, with peak separation dictated as much by inner-sphere substrate binding and film structure as by the underlying electron-transfer rate [77–80,82–84]. Reported k° for the isolated Co^{2+}/Co^{3+} step falls within 10^{-3}–10^{-2} cm s^{-1} and often decreases upon repeated cycling due to partial demetalation, axial-ligand exchange or macrocycle oxidation [80,82–84]. In supramolecular cobalt coordination polymers, the formal Co^{2+}/Co^{3+} couple remains visible but is superimposed on pronounced catalytic currents, and apparent

diffusion coefficients extracted from hopping models are one to two orders of magnitude lower than those of classical outer-sphere mediators [15,81,85–87]. Overall, cobalt centres in biosensing films operate as quasi-reversible systems whose voltammetric profiles are dominated by inner-sphere chemistry, film microstructure and catalytic EC′ pathways; the Co^{2+}/Co^{3+} couple can therefore support efficient peroxide-based signalling but is poorly suited as a benchmark reversible mediator [15,81,85–87].

Cobalt phthalocyanines and tetraphenylporphyrins remain the most widely studied cobalt mediators and function as surface-bound inner-sphere redox centres that mediate H_2O_2 or substrate oxidation via an EC′ mechanism [78,79]. A covalently linked pentamer, **8**–(**9**)$_4$, immobilised on glassy carbon, exhibits a well-defined Co^{2+}/Co^{3+} couple in neutral and alkaline media and catalyses H_2O_2 reduction with low micromolar detection limits and fast chronoamperometric responses without dissolved mediator [79]. The same pentamer mediates glucose oxidation efficiently by accepting electrons from glucose oxidase (GOx)-generated H_2O_2 at substantially lower potentials than bare carbon [78]. Self-assembled tetracarboxylic cobalt phthalocyanine monolayers also display a stable quasi-reversible Co^{2+}/Co^{3+} wave and robust H_2O_2 electrocatalysis. However, performance depends strongly on monolayer order, the axial-ligand environment, and the accessibility of the Co centre [77]. Fluorinated or polymeric cobalt phthalocyanines on carbon supports exhibit similar behaviour, with enhanced dispersion and tuned potentials, but remain dominated by inner-sphere peroxide reduction rather than pure outer-sphere mediation [80,81].

Beyond discrete macrocycles, cobalt-based supramolecular coordination polymers serve as both immobilisation scaffolds and redox-active mediator networks. The Co^{2+} coordination polymer **10** is a representative example: it co-immobilises GOx on glassy carbon in a single casting step, displays a quasi-reversible Co^{2+}/Co^{3+} couple under neutral aqueous conditions and participates directly in an EC′ catalytic cycle where GOx-generated H_2O_2 oxidises Co^{2+} to Co^{3+}, and the electrode subsequently reduces the film [82]. Although CV and spectroscopy show that structural changes during cycling are modest and the response remains stable, the mechanism remains non-Nernstian and dominated by catalytic peroxide turnover [82]. Mixed-ligand cobalt complexes embedded in conducting polymers or CNT composites have similarly been used to mediate ET in glucose and H_2O_2-based sensors, but in nearly all cases, the mechanism reflects a combination of inner-sphere mediation and electrocatalysis rather than clean outer-sphere shuttling [83,85].

Cobalt-based mediators present several constraints relative to osmium, ruthenium and low-potential organic systems. Their Co^{2+}/Co^{3+} potentials (0.0 to 0.30 V vs. Ag/AgCl) do not promote oxygen reduction but overlap the anodic onset of endogenous interferents such as ascorbate, urate and phenolic metabolites, with catalytic EC′ turnover further shifting operating bias positive and increasing susceptibility to non-specific oxidation [78,82]. Cobalt macrocycles may undergo gradual demetalation, ligand oxidation or axial substitution during repeated cycling, leading to drift in peak position and diminished mediator capacity [80,86]. Polymer-supported cobalt systems improve retention but still experience partial loss of electroactivity due to film rearrangement or ion-transport limitations in hydrated matrices [82]. Finally, multistep synthesis and purification requirements for cobalt macrocycles render high-loading disposable sensors less economical than Fc- or quinone-based platforms [15,77]. These factors position cobalt mediators as valuable but specialised redox systems, best employed when their coordination chemistry or surface-binding properties confer functional advantages that lower-potential or more reversible mediator classes cannot.

3. Organic Mediators: Limits and Mechanistic Contrast

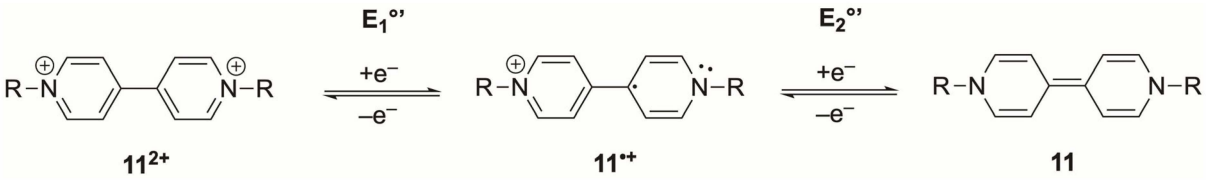
Organic mediators occupy a chemically diverse and electrochemically expansive domain, ranging from the deeply reducing viologens to the more oxidising aminophenol and indophenol derivatives. Although these systems offer tuneable potentials and, in some cases, fast electron-transfer kinetics, their apparent reversibility is governed as much by chemical stability as by intrinsic redox behaviour. Unlike organometallic and inorganic mediators, whose cycling is stabilised by rigid ligand fields and predictable outer-sphere mechanisms, most organic redox couples are embedded within proton-coupled electron-transfer manifolds, hydration equilibria, tautomerisation pathways and structural rearrangements that compete directly with electrode-driven cycling [2,88].

As a result, even when CVs appear Nernstian over limited timescales, the oxidised or reduced forms of many organic mediators undergo side reactions, such as hydration, semiquinone formation, Michael-type addition, radical dimerisation or polymerisation, that progressively erode true reversibility in aqueous media. These chemical constraints define the limits within which organic mediators can operate reliably and highlight the mechanistic contrasts that motivate the transition to metal-centred systems in long-term biosensing applications [18,89,90].

The following subsections examine prominent organic mediator families, including viologens, phenazines, quinones, catechols, indophenols, aminophenols, azines, phenothiazines and phenoxazines, emphasising the structural, proton-coupled and microenvironmental factors that govern their stability and effective reversibility under operational conditions.

3.1. Viologens

Viologens, the 4,4′-bipyridinium family of redox-active molecules, represent one of the most extensively characterised classes of organic mediators in electrochemistry. Their widespread use in early and contemporary biosensors stems from the intrinsic reversibility of the $\mathbf{11^{2+}/11^{\bullet+}}$ couple (Scheme 1), the ease with which their formal potentials can be tuned, and the compatibility of the bipyridinium scaffold with numerous immobilisation strategies [91]. The parent dication $\mathbf{11^{2+}}$ undergoes two sequential one-electron reductions, first to the persistent blue radical cation $\mathbf{11^{\bullet+}}$ and then to the neutral species **11**, a stepwise two-ET pattern described in classical electroanalytical treatments [18,92]. These well-defined redox transitions have made viologens benchmark systems for validating electrode surfaces and for constructing controlled electron-transfer pathways in biosensors and redox polymers.



Scheme 1. General mechanism for the two-step reduction of viologens, where R denotes the N-substituent, and $E_1^{\circ\prime}$ and $E_2^{\circ\prime}$ are the formal potentials for the first ($\mathbf{11^{2+}/11^{\bullet+}}$) and second ($\mathbf{11^{\bullet+}/11}$) one-electron couples.

Although viologens can store two electrons, the two redox steps are not concerted and typically differ by several hundred millivolts. For example, in acetonitrile containing 0.1 M $[Bu_4N][PF_6]$ as the supporting electrolyte, methyl viologen displays $E_1^{\circ\prime} = -0.76$ V and $E_2^{\circ\prime} = -1.18$ V vs. Ag/Ag^+, giving a separation of ca. 0.42 V [93,94]. In aqueous media, substituted viologens likewise show well-separated couples. In 1 M Na_2SO_4, the $E_1^{\circ\prime}$ typically appears around −0.61 V vs. Ag/AgCl, 3 M NaCl and $E_2^{\circ\prime}$ near 0.3 V more

negative than $E_1^{\circ\prime}$, which varies only modestly with N-substitution [95]. In biosensing, only the first, well-behaved $\mathbf{11^{2+}/11^{\bullet+}}$ transition is exploited: it lies within the potential range of biological cofactors and avoids generating the neutral species **11**, which is strongly adsorbing and chemically unstable under aerobic conditions [95]. Thus, viologens operate functionally as one-electron mediators despite their formal two-electron capacity.

Under inert conditions and at moderate scan rates, the $\mathbf{11^{2+}/11^{\bullet+}}$ couple of soluble viologens typically exhibits ΔE_p values very close to the Nernstian 59 mV limit for a one-electron process, with $i_{pa}/i_{pc} \sim 1$, reflecting fast heterogeneous ET and classical electrochemical reversibility on glassy carbon, gold, and carbon-based surfaces [96,97]. These features are consistently observed in both aqueous and non-aqueous media, and the behaviour remains near-Nernstian across 0.01–0.10 V s^{-1}.

Quantitative analysis using Nicholson, Matsuda–Ayabe or Laviron formalisms typically yields k° in the range 10^{-3}–10^{-1} cm s^{-1}, depending on substitution, counter-ion and electrode surface [98,99]. For $k^\circ \geq (3\text{–}5) \times 10^{-2}$ cm s^{-1}, the first $\mathbf{11^{2+}/11^{\bullet+}}$ reduction behaves electrochemically reversible ($\Lambda \geq 15$ at v of ca. 0.05–0.10 V s^{-1}), whereas systems with k° closer to 10^{-3}–10^{-2} cm s^{-1} fall into the quasi-reversible regime. This spread is consistent with canonical descriptions of viologen electrochemistry, where many derivatives exhibit near-Nernstian behaviour under typical biosensor conditions.

Departures from ideal reversibility arise from well-documented chemical side processes, particularly radical–radical dimerisation, surface adsorption, and oxygen-mediated redox cycling. Radical dimerisation has measurable kinetics and leads to broadened or distorted waves with increased ΔE_p and progressive cycling drift [96,97]. Adsorption of the reduced species at carbon surfaces likewise generates asymmetric peak shapes and quasi-reversible character over repeated scans [98]. In aerated solutions, rapid mediated oxygen reduction through the $\mathbf{11^{2+}/11^{\bullet+}}$ cycle perturbs voltammetry, increases apparent currents and accelerates chemical degradation of the mediator [100,101].

When viologens are immobilised in redox polymers or tethered films, the electrochemical response transitions to surface-confined waves with ΔE_p remaining close to ~60 mV even at scan rates up to several hundred mV s^{-1}, indicative of fast intrafilm electron hopping and efficient charge transport [102,103]. The shift from diffusion-limited to ion-transport-limited behaviour at higher scan rates highlights the role of ionic mobility within the matrix, which becomes the rate-determining step rather than ET itself.

In practice, therefore, viologen-based mediators are electrochemically reversible on the timescales and potential windows relevant to biosensing. Their practical long-term reversibility is governed not by intrinsic electron-transfer kinetics but by radical stability, oxygen sensitivity, adsorption phenomena and the physicochemical architecture of the host film (hydration, thickness, ion-mobility constraints) [99,103].

N-alkyl substitution produces only modest (tens of millivolts) shifts in $E_1^{\circ\prime}$, whereas aromatic ring substitution allows much larger and systematic tuning of viologen redox thermodynamics [104]. Electron-withdrawing cyano groups shift $E_1^{\circ\prime}$ to more positive values and stabilise $\mathbf{11^{\bullet+}}$, as demonstrated for mono- and dicyanoviologens [105]. In aqueous 0.1 M phosphate buffer (pH 7.4) with Ag/AgC, 3 M KCl reference, introduction of a single cyano group moves the first redox wave from ca. −0.65 to −0.34 V, and the dicyano derivative undergoes a further positive shift to $E_1^{\circ\prime}$ = 0.06 V [32]. These shifts provide a direct means of placing the $\mathbf{11^{2+}/11^{\bullet+}}$ couple well above typical flavin potentials.

In contrast, and as mentioned before, variation in the N-substituent around the viologen core enables fine-tuning within negative-potential regimes. An aqueous library encompassing non-polar, anionic and cationic substituents showed $E_1^{\circ\prime}$ = −0.54 to −0.67 V vs. Ag/AgCl, with benzyl viologen centred near −0.54 V [106]. Extended aromatic and long-chain alkyl groups promote π-π stacking and amphiphilic behaviour, favouring or-

dered packing and aggregate formation in solution and at interfaces, whereas strongly polar or sulfonated substituents enhance water solubility of both redox states and suppress radical-radical dimerisation [91,107–109]. These substituent effects collectively provide a molecular basis for tuning viologen potentials to match enzymatic cofactors while retaining reversible electrochemical behaviour.

Polymer-tethered viologens extend these design principles by fixing the mediator within a redox-active matrix. Pendant dicyanoviologen units embedded in a hydrophilic methacrylate-type backbone undergo rapid electron hopping, enabling efficient communication between FAD-GDH active sites and the electrode [105]. In neutral phosphate buffer, the free dicyanoviologen monomer displays $E_1{}^{\circ\prime}$ = 0.06 V, whereas the drop-cast polymer film shows a slightly less positive potential at ca. 0.05 V, with minimal pH dependence [20]. The polymer retains well-defined peaks during extended cycling and supports stable catalytic glucose oxidation, illustrating how cyano substitution combined with polymer confinement tunes $E_1{}^{\circ\prime}$, stabilises the radical cation and suppresses mediator loss.

Complementary work on amphiphilic and surface-anchored viologens shows how nanoscale organisation governs electron-transfer behaviour. Langmuir–Blodgett multilayers and self-assembled films formed from long-chain or sulfonated viologens impose structural order, with packing density, tilt angle and film thickness exerting strong control over reversibility and accessible electron-transfer distances [91,107–109]. In such supramolecular architectures, the $\mathbf{11}^{2+}/\mathbf{11}^{\bullet+}$ couple typically resides within −0.4 to −0.6 V vs. Ag/AgCl, but kinetic parameters vary markedly with film organisation.

The redox potential of the $\mathbf{11}^{2+}/\mathbf{11}^{\bullet+}$ couple is well-suited to ET from reduced flavins, enabling efficient coupling with FAD-dependent oxidases and dehydrogenases. Methyl viologen readily accepts electrons from $FADH_2$ in GOx systems, underpinning its historical use in first-generation glucose sensors [91,107]. Dicyanoviologen polymers couple efficiently with FAD-GDH, allowing the oxidation of $FADH_2$ at potentials substantially lower than those for oxygen reduction [105]. Benzyl viologen's potential near −0.54 V matches the unusually low redox potential of F420, enabling reversible cofactor cycling with minimal overpotential [105]. These examples underscore that viologen functionality is determined by the mediator's tuneable potential landscape rather than by the enzyme itself.

Despite their excellent electrochemical reversibility, viologens exhibit several chemical limitations relevant to biosensor design. The radical cation $\mathbf{11}^{\bullet+}$ can undergo disproportionation or dimerisation at high surface coverage or in poorly hydrated films, perturbing voltammetry at slow scan rates [18]. The fully reduced species **11** strongly adsorbs onto carbon electrodes, leading to quasi-reversible behaviour and hysteresis. The $\mathbf{11}^{\bullet+}$ intermediate reacts rapidly with dissolved O_2 to form superoxide, regenerating $\mathbf{11}^{2+}$, as evidenced in methyl viologen/Nafion films where O_2 reduction dominates the background current [107]. Light exposure can induce photoreduction, particularly in viologen films containing chromophoric groups or photoactive co-components [108]. These pathways illustrate that viologens are electrochemically reversible but chemically fragile under certain conditions, underscoring the importance of immobilisation, film hydration, and control of O_2 or light exposure.

Toxicity represents an additional constraint. Methyl viologen is the herbicide paraquat, whose well-documented toxicity stems from efficient redox cycling with molecular oxygen to generate reactive oxygen species [110]. Although viologens in general share the capacity to form persistent radical cations, the extent of biologically relevant redox cycling varies with substitution pattern, hydrophobicity and membrane permeability. Free viologens can therefore exhibit reactive oxygen species-associated cytotoxicity when sufficiently bioavailable, whereas immobilisation within polymers, hydrogels or Nafion restricts diffusion and cellular uptake, substantially mitigating these risks. Consequently, toxicity consider-

ations remain essential for in vivo or environmental applications, motivating the use of immobilised mediators over freely diffusing ones.

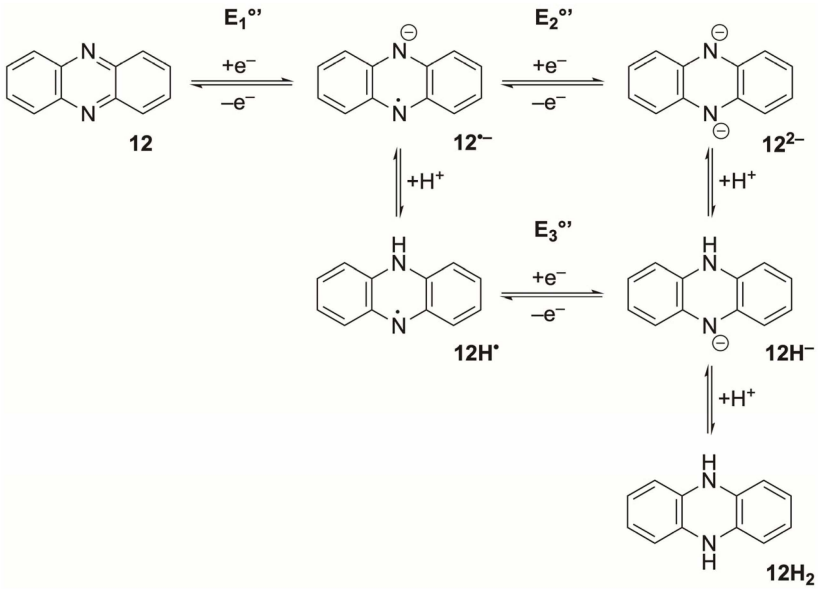
Together, these insights establish clear design principles for constructing viologen-based mediators with high practical reversibility. Substituent chemistry should be selected to stabilise the $\mathbf{11}^{\bullet+}$ state, minimise pathways that compromise chemical reversibility (dimerisation, disproportionation, O_2 reactivity) and position the $\mathbf{11}^{2+}/\mathbf{11}^{\bullet+}$ couple within a useful biological potential window. Polymer-tethered architectures and immobilised matrices should be prioritised, as confinement suppresses mediator loss, moderates radical side reactions, and preserves near-Nernstian behaviour over repeated cycling. Control of film hydration, counter-ion mobility and nanoscale organisation is essential, since these parameters dictate whether the system remains in the reversible regime or drifts towards quasi-reversible behaviour. Collectively, these strategies translate the intrinsic electrochemical reversibility of viologens into robust, long-lived mediator performance suitable for biosensing applications.

3.2. Phenazines

Phenazines form a second major family of low-potential organic mediators whose electrochemical behaviour depends strongly on substitution at the ring nitrogens. The parent phenazine (**12**) undergoes a proton-coupled ECEC mechanism (a four-step redox process consisting of alternating electrochemical (E) and chemical (C) steps) in aqueous media (Scheme 2) [111,112]: the first ET produces a radical anion ($\mathbf{12}^{\bullet-}$) that is rapidly protonated, followed by a second ET and protonation to yield the dihydrophenazine ($\mathbf{12H_2}$). This pathway generates two pH-dependent, often broadened one-electron waves and commonly exhibits adsorption and non-Nernstian behaviour, particularly on carbon electrodes [113,114]. In contrast, N,N′-substituted phenazines such as phenazine methosulfate (PMS) and phenazine ethosulfate (PES) cannot undergo protonation at the ring nitrogens and instead display a clean, pH-insensitive two-electron reduction. Although these derivatives appear to undergo a single $2e^-$ process, the underlying mechanism is not a concerted EE step. Rather, blocking protonation collapses the usual ECEC sequence of the parent phenazine into two sequential electron-transfer steps ($E_1°'$ and $E_2°'$) whose formal potentials differ by only a few millivolts; as a result, the two $1e^-$ waves merge into a single voltammetric feature that behaves as a reversible $2e^-$ couple. In aqueous buffer, these derivatives typically show a single, well-defined $2e^-$ wave centred at -0.05 to -0.10 V vs. Ag/AgCl, with fast heterogeneous ET and minimal peak separation [115,116]. Substitution at the N-positions also suppresses formation of protonated semiquinone-type intermediates and improves chemical stability relative to the free phenazine scaffold, whose reduced forms readily undergo follow-up chemistry and surface adsorption [117,118]. These mechanistic distinctions align with general treatments of proton-coupled ET and mediator-based electrochemical catalysis, in which blocking protonation pathways collapses multi-step ECEC sequences into reversible electron-transfer waves [90,119].

Under conditions relevant to biosensing, N-substituted phenazines such PMS and PES typically display high quasi-reversible to reversible behaviour on voltammetric timescales. Cyclic voltammograms of PMS and PES in buffered aqueous media show single, well-defined redox waves with small peak separations and formal potentials near -0.22 V and -0.19 V vs. Ag/AgCl, 3 M NaCl, respectively, at pH 8–8.5 [120]. The analysis of the $\mathbf{12}/\mathbf{12H_2}$ couple indicates that ET at the electrode can be intrinsically fast, with apparent surface rate constants of 10^6–10^7 s^{-1} for adsorbed species [89]. Solution-phase studies in aprotic media similarly report $k°$ in the 10^{-2}–10^{-1} cm s^{-1} range [121], placing the first reduction step in the Matsuda–Ayabe high quasi-reversible to reversible regime under typical CV scan rate (0.05–0.10 V s^{-1}). Deviations from ideal Nernstian behaviour in aque-

ous solution arise mainly from proton-coupled follow-up chemistry, modest adsorption of reduced species and the chemical reactivity of the **12H$_2$** form, which increases ΔE_p and introduces minor scan-rate dependence [89,122,123]. Phenazine methosulfate additionally undergoes oxygen-driven autoxidation and light-induced decomposition, forming secondary phenazine products that contribute to current drift, whereas PES is comparatively more photochemically stable [120,124,125]. In immobilised formats, such as PES-based redox hydrogels, covalently tethered phenazine derivatives or phenazine-bearing redox polymers, the redox response becomes surface-confined, with narrow peak separations even at elevated scan rates, reflecting fast segmental electron hopping and the suppression of mediator-loss pathways [113,126,127]. Overall, phenazines exhibit electron-transfer reversibility that is primarily limited by chemical instability rather than by slow electrode kinetics, making them effective short-timescale mediators when photodegradation and oxygen exposure are controlled.



Scheme 2. Stepwise reduction of phenazine (**12**). Electron-transfer steps proceed horizontally, while protonation steps occur vertically.

Substitution both at the phenazine core and on the sulfonate/sulfate side chains allows further tuning of solubility, aggregation and the formal potential. Phenazine methosulfate and PES, which are the most widely used mediators in biosensing, are cationic salts with high aqueous solubility. In contrast, more hydrophobic or extended-aromatic phenazine derivatives can be incorporated into polymer matrices or sol-gel films. Electropolymerised PMS films and phenazine-containing redox polymers demonstrate that phenazine units can be immobilised while retaining quasi-reversible ET; the polymer environments facilitate rapid electron hopping and minimise mediator loss during cycling [114,117]. In inorganic composite electrodes such as TiO_2-based systems, thin PMS layers act as surface-confined mediators that efficiently relay electrons between the electrode and dissolved H_2O_2 or enzymatically generated intermediates, yielding well-defined surface waves and stable amperometric signals [115,118]. Recent PMS- and PES-modified carbon electrodes and polymer composites show that immobilisation stabilises the two-electron wave, reduces photodegradation and improves long-term operational stability under continuous turnover [113].

Functionally, phenazines have been applied most broadly to dehydrogenase- and oxidase-based biosensors operating at low potentials. Phenazine methosulfate and PES are established mediators for NAD^+-dependent dehydrogenases, shuttling electrons from

enzymatically produced NADH to the electrode. This strategy has been used in sensors for lactate, glutamate, ethanol, malate and glucose, where the relatively positive potential of PMS enables efficient NADH oxidation without requiring large overpotentials that would increase interference from endogenous reductants [114,116]. Phenazine-modified electrodes have also been used to wire FAD-dependent and PQQ-dependent enzymes, as well as to couple peroxidase-type reactions to H_2O_2 detection at low potentials, improving selectivity in oxidase-based biosensors [113,115]. More recent computationally guided work has produced substituted phenazine analogues designed to stabilise the radical intermediate and shift the $2e^-$ wave into a more biologically compatible potential window, enabling extended linear ranges and improved interference tolerance in whole-blood glucose sensing [8]. These developments reflect broader principles of mediator design in electroenzymatic systems, where matching mediator potential to cofactor thermodynamics and ensuring rapid interfacial exchange are essential for achieving efficient catalytic currents [119].

Phenazines also present several limitations relevant to biosensor design. Reduced PMS and PES autoxidise readily in the presence of dissolved oxygen, forming superoxide and regenerating the oxidised mediator; while this redox cycling can enhance apparent catalytic efficiency, it also elevates background currents and produces reactive oxygen species that may degrade enzymes or biological analytes during prolonged operation [114,118]. Under strongly reducing conditions, reduced phenazines may dimerise or irreversibly adsorb onto carbon electrodes, gradually diminishing reversibility and contributing to electrode fouling [117]. Photosensitivity is another concern: several substituted phenazines bleach or degrade under illumination, particularly in transparent-electrode or optical-sensor formats [113]. Finally, like viologens, phenazines exhibit intrinsic toxicity through redox cycling and reactive oxygen species generation; this necessitates immobilised, polymer-confined or membrane-separated architectures for biological or environmental applications that involve sustained exposure.

Taken together, phenazines complement viologens as tuneable low-potential mediators. Their proton-coupled redox chemistry, the clean two-electron behaviour of N-substituted derivatives, and their strong compatibility with NAD-dependent dehydrogenases make them particularly valuable for low-potential bioelectrocatalytic systems. Polymer-tethered, immobilised, and composite-film implementations mitigate issues of autoxidation, fouling and toxicity, enabling phenazines to operate effectively in continuous-monitoring sensors and biofuel cells.

3.3. Quinones and Catechols

Quinones (**13** and **14**, Figure 4) and their reduced catechol/hydroquinone counterparts span a broad low-to-mid-potential window, reflecting strong substituent-dependent modulation of redox thermodynamics. In neutral buffered aqueous media, typical $2e^-/2H^+$ formal potentials for the benzoquinone/hydroquinone couple fall roughly between −0.30 and 0.3 V vs. Ag/AgCl, 3 M NaCl, depending on ring size, substitution, and pH [128,129]. Simple 1,4-benzoquinone and 2,3,5,6-tetramethyl-1,4-benzoquinone cluster near −0.21 to −0.16 V vs. Ag/AgCl, 3 M NaCl at pH 7 [76,128], while mono- and dihydroxynaphthoquinones (Figure 4) lie slightly more positive, between −0.08 and −0.06 V vs. Ag/AgCl, 3 M NaCl [128]. More extended π-systems such as anthraquinone-1,5-disulfonate exhibit considerably lower potentials of ca. −0.91 V vs. Ag/AgCl, 3 M NaCl [128], and anthraquinone-2-sulfonate sits near −0.44 V vs. Ag/AgCl, 3 M NaCl in neutral media [130]. Thus, by progressing from benzo- to naphtho- to anthraquinones (Figure 4), one can systematically shift the working potential from slightly positive to moderately negative values while retaining the same basic quinone/hydroquinone redox motif.

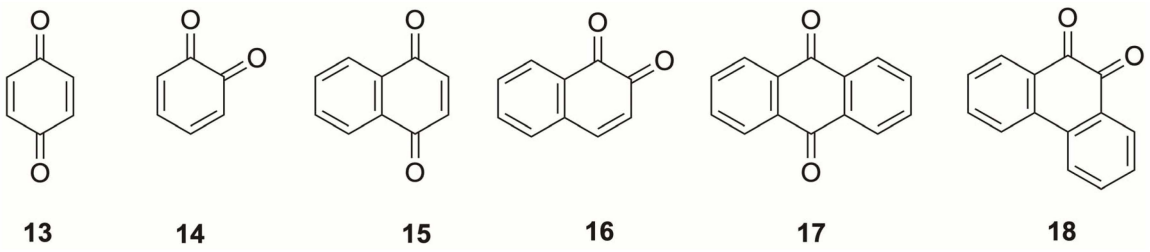
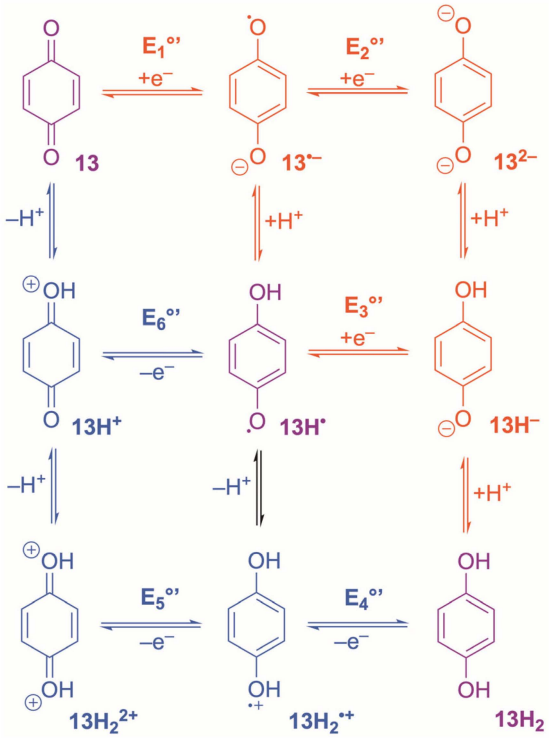


Figure 4. Representative parent structures of quinones showing progressive ring extension: (**13**) 1,4-benzoquinone, (**14**) 1,2-benzoquinone, (**15**) 1,4-naphthoquinone, (**16**) 1,2-naphthoquinone, (**17**) 9,10-anthraquinone, and (**18**) 9,10-phenanthraquinone.

Electrochemically, quinones behave as classic PCET systems. In protic media, reduction of quinone to hydroquinone (Scheme 3) usually proceeds through two sequential $1e^-/1H^+$ steps, often appearing as an apparently concerted $2e^-/2H^+$ wave when the formal potentials ($E_1°'$ and $E_3°'$) collapse [5,90]. At moderate scan rates, benzo- and naphthoquinones frequently display near-Nernstian ΔE_p values of 60–70 mV [129]. Yet, the oxidised quinone (**13**) is chemically fragile: hydration, Michael addition, and polymerisation occur readily under neutral or basic conditions [5,90,131–134], compromising long-term reversibility even when CV appears ideal over short timescales. In contrast, the reduced hydroquinone, **13H$_2$**, is typically more resistant to decomposition because the aromatic ring is deactivated toward nucleophiles and stabilised by hydrogen bonding or solvation [5,90,131–134]. Consequently, many quinone systems are best viewed as fast-kinetic, quasi-reversible couples that appear reversible over short timescales but are chemically limited.



Scheme 3. Bidirectional proton-coupled electron-transfer mechanism for the benzoquinone/hydroquinone couple. Red arrows show the reduction sequence ($E_1°'$–$E_3°'$); blue arrows show the reverse oxidation pathway ($E_4°$–$E_6°$). Horizontal steps denote ET, and vertical steps denote proton transfer. Purple structures are common to both directions.

Across the quinone family, electron-transfer kinetics are generally fast, but the degree of electrochemical reversibility depends strongly on PCET and the stability of the semiquinone (**13H$^{\bullet}$**) intermediate. In aqueous media, **13**/**13H$_2$** couples typically display near-Nernstian behaviour with ΔE_p values approaching 59 mV at moderate scan rates when proton transfer is rapid and well coupled to ET, consistent with stepwise ECEC-type PCET mechanisms [135]. Catechols and substituted hydroquinones frequently show ΔE_p between 60–80 mV on glassy carbon at 25 °C, with i_{pa}/i_{pc}~1 and minimal scan-rate dependence, reflecting k° in the 10^{-3}–10^{-2} cm s^{-1} range [136,137]. These values place typical quinone couples firmly in the quasi-reversible regime under usual aqueous CV conditions, with apparent reversibility improving only when proton transfer is fast and chemical steps remain in pre-equilibrium [138,139].

Departures from ideal behaviour arise primarily from chemical rather than electron-transfer limitations. Semiquinones can undergo disproportionation, proton-loss equilibria, or oxygen-driven radical chemistry, leading to broadened peaks, elevated ΔE_p, or loss of cyclic stability, particularly on carbon electrodes [135,140]. Adsorption also plays a significant role: many catechols and polyaromatic quinones interact strongly with graphitic surfaces, giving rise to surface-confined signatures, increased peak currents, and Laviron-type scan-rate scaling rather than pure diffusion control [136,137]. Under such conditions, ET remains rapid, but the apparent electrochemical reversibility becomes modified by interfacial ordering and ion-transport limitations.

Immobilised and polymer-bound quinones often exhibit more symmetric and kinetically improved voltammetry than freely diffusing quinones, although the peak separations observed (typically 55–70 mV) still place these systems in the high quasi-reversible regime rather than fully reversible 2e$^-$ behaviour. Phenanthrenequinone- and phenanthroline-5,6-dione-based redox films show relatively narrow peak separations, enhanced cycling stability, and well-defined surface-confined responses with fast intrafilm electron-hopping processes [141–143]. Electropolymerised quinone coatings and nanostructured phenanthrenequinone films similarly display quasi-reversible voltammetry even at elevated scan rates, reflecting rapid interfacial ET and the suppression of semiquinone-decay pathways afforded by the immobilised environment [144,145]. Collectively, these observations indicate that immobilisation mitigates many of the chemical and interfacial processes that broaden quinone waves in solution, leading to near-reversible cycling behaviour on the timescales relevant to biosensing, even though the fundamental electrochemical response remains quasi-reversible for a nominal 2e$^-$ couple.

Substituent effects provide a straightforward path to tuning both potential and stability. Electron-withdrawing groups (e.g., halogens, sulfonates, carbonyls) shift the formal potential to more positive values and often enhance autoxidation or nucleophilic attack [146]. Electron-donating groups (e.g., methyl, methoxy, amino) shift the formal potential to more negative values and reduce the electrophilicity of quinones, improving robustness [76]. In systematic mediator screens for GDH, tetramethyl-1,4-benzoquinone displayed $E^{\circ\prime}$ of ca. −0.2 V vs. Ag/AgCl, 3 M NaCl, whereas chloro- and sulfonated quinones shifted the $E^{\circ\prime}$ 0.05–0.15 mV more positive [146]. Extended systems, such as anthraquinone-2-sulfonate, similarly illustrate that combining a rigid π framework with electron-withdrawing substituents yields low-potential shuttles suitable for NADH-based catalysis [130].

Catechol-type mediators share the same underlying PCET landscape (Scheme 3). Their oxidation to o-quinones often appears quasi-reversible because proton-transfer kinetics and semiquinone disproportionation compete with ET [129]. In buffered systems, reversibility improves as proton availability increases, but autoxidation routes, leading to semiquinone radicals and melanin-like polymers, can still limit cycling stability [129]. Synthetic catechol/quinone-imines such as 2,6-Dichlorophenolindophenol behave similarly,

exhibiting mid-potential redox couples around 0.0–0.1 V vs. Ag/AgCl that are sufficiently positive to oxidise reduced flavins while avoiding substantial oxygen interference [147].

Immobilisation strategies mirror those used for viologens and phenazines. Quinones and catechols can be covalently grafted onto polymer backbones (e.g., styrene, methacrylate, phenanthroline) [9,148], electropolymerised from quinone-bearing monomers [147], or co-assembled with carbon materials, porous carbons, or metal oxides [148,149]. Anthraquinone-sulfonate layers on carbon cloth and CNTs act as robust low-potential shuttles in biofuel cells and microbial electrochemical systems [76,130]. Confinement within hydrophobic or partially shielded microenvironments decreases access of nucleophiles and oxygen, suppressing side reactions and improving apparent reversibility over extended cycling [9,148].

From a biosensing standpoint, quinones and catechols are most often paired with NAD-dependent dehydrogenases and flavin enzymes. Benzoquinone, tetramethylbenzoquinone, naphthoquinones and anthraquinone sulfonates have been used as mediators for sensors targeting glucose, lactate, malate, alcohols and other substrates, in which quinones accept electrons from NADH and reoxidise at the electrode in the 0.0 to −0.3 V vs. Ag/AgCl window [9,128]. Quinone-functionalised redox polymers can wire FAD- or PQQ-dependent oxidases, enabling low-potential operation with enhanced selectivity over oxygen [148,149]. Catechol/quinone imines, such as 2,6-dichlorophenolindopheno, are widely used with FAD-GDH in glucose sensors, where their mid-positive potentials support efficient $FADH_2$ oxidation and high operational stability [147].

Limitations reflect the same PCET chemistry: oxidised quinones undergo nucleophilic attack, hydration and polymerisation, rapidly degrading at neutral or basic pH [128]. Under operational conditions, oxygen-driven radical pathways continue to contribute to signal drift and reduced sensor longevity, particularly for catechol-derived mediators [129,147]. Biologically active quinones (e.g., menadione) pose toxicity concerns, favouring immobilised or membrane-separated architectures for clinical or environmental applications [128]. Nonetheless, when properly tuned and stabilised, quinones and catechols offer a versatile mid-potential platform bridging low-potential organic mediators and higher-potential metal complexes.

Classical hydroquinone/benzoquinone reporters used in early HRP assays exemplify these limitations. Even in well-defined acidic media, the couple can display near-reversible behaviour, but at neutral pH, PCET introduces intrinsic quasi-reversibility, and chemical instability further degrades performance: hydroquinone undergoes autoxidation, and benzoquinone readily participates in nucleophilic addition and polymerisation. These combined kinetic and chemical complications produce signal drift and a gradual loss of analytical response. Such issues contributed to the shift toward lower-potential aminophenol reporters, whose redox chemistry provides a cleaner amperometric readout and improved operational stability in biosensing contexts [2].

3.4. Aminophenol and Indophenol Derivatives

Within the upper region of the organic potential window lie the aminophenol and indophenol derivatives (Figure 5), two families that span similar potential ranges but differ fundamentally in their thermodynamic roles, mechanistic behaviour, and chemical stability. Indophenol dyes act as oxidising mediators through well-defined $2e^-/2H^+$ proton-coupled ET, whereas aminophenols function as reducing mediators whose oxidation proceeds through an ECEC sequence to quinone-imines rather than through a Nernstian redox couple. The formal potential of **19** lies between 0.27 and 0.28 V vs. Ag/AgCl at pH 5 and from 0.03 to 0.16 V at pH 9 on carbon electrodes, with mass-transport-limited currents above approximately 0.35 V, although biosensing applications typically operate

between 0.10 and 0.38 V, below the oxidation of ascorbate, urate, paracetamol and other endogenous interferents [150,151]. When **19** is confined within carboxylated self-assembled monolayers on gold, the voltammetric profile becomes sharper, exhibiting ΔE_p~45 mV, faster kinetics and an anodic shift of roughly 0.10 V, reflecting electrostatic preconcentration rather than genuine chemical reversibility [87]. In all systems, **19** oxidation follows an ECEC pathway (Scheme 4): an initial one-electron oxidation generates the aminophenoxyl radical cation (**19**$^{\bullet+}$), which undergoes rapid deprotonation to form the O-centred radical (**19H**$^{\bullet}$). A second electron-transfer step converts this species into the p-quinone-imine cation (**19H**$^{+}$), followed by deprotonation to the neutral quinone-imine (**19-QI**) and subsequent hydrolysis to p-benzoquinone (**13**). The quinone-imine does not vanish immediately but undergoes slow hydrolysis on the timescale of minutes, yielding **13** and ammonium, a process confirmed by the appearance of quinone carbonyl bands and NH_4^+ in spectroscopic studies [151,152]. The newly formed **13** is itself a mid-potential $2e^-/2H^+$ PCET mediator, meaning the mediator pool shifts over time from an aminophenol ECEC regime into a classical quinone/hydroquinone couple rather than being irreversibly lost. This kinetic partitioning allows **19** to function effectively in short-timescale amperometric assays, where the quinone-imine persists long enough to support reliable reporting, while progressive hydrolysis during longer incubations produces time-dependent changes in catalytic onset potential, background current and interference behaviour. N-acylated aminophenols shift the $E^{\circ\prime}$ into 0.55–0.60 V region and suppress radical–radical coupling to a degree, yet their quinone-imine products still enter the benzoquinone pathway. This highlights that long-term mediator stability is governed more by the extended measurement window over which downstream chemical reactions accumulate than by the initial electron-transfer event.

The ortho and meta isomers diverge even more strongly from reversible mediator behaviour. The o-aminophenol (**20**) yields aminophenoxazinone dimers that propagate into conjugated phenoxazine ladder polymers, producing stable, electroactive surface films that alter electrode characteristics and consume monomer [152,153]. Meanwhlile, m-aminophenol predominantly forms crosslinked or ether-linked oligomers with low conductivity, rapidly fouling the electrode and terminating turnover [152]. Newly incorporated studies of m-aminophenol in HRP assays illustrate an alternative mechanistic route in enzymatic contexts: HRP does not oxidise m-aminophenol to a simple meta-quinone-imine; instead, it promotes radical–radical coupling to yield the dimeric cyclohexadienedione derivative 2-amino-5-(3-hydroxyphenyl)amino-2,5-cyclohexadiene-1,4-dione. This product exhibits a well-defined, reversible $2e^-/2H^+$ PCET couple at approximately -0.43 V vs. Ag/AgCl from pH 5 to 12, with a -67 mV pH^{-1} shift consistent with a quinone-like $2e^-$ redox process [154]. This behaviour reinforces the microenvironmental sensitivity of aminophenol chemistry. Whereas **19-QI** hydrolyse rapidly under typical biosensing conditions, the HRP-generated m-aminophenol coupling product forms a far more stable cyclohexadienedione species that persists on the timescale of minutes, which is sufficiently long-lived to function as an electroactive reporter.

Despite their fast electron-transfer kinetics and near-reversible voltammetric signatures at short timescales, aminophenols are chemically irreversible mediators because the oxidised quinone-imine rapidly undergoes follow-on reactions rather than establishing a stable redox couple. Even when **19** displays relatively small peak separations on carbon electrodes, ΔE_p values ranging from ca. 140 mV on untreated glassy carbon to 60–70 mV on thermally pretreated electrodes, and as low as ~39 mV on optimised plasma-treated screen-printed carbon electrodes, this "near-reversible" appearance arises from rapid ECEC kinetics rather than a Nernstian EE process [155]. Quantitative spectroelectrochemical studies demonstrate that **19-QI** formed after the second ET is chemically short-lived: it hydrolyses to **13** with a pseudo-first-order rate constant of 0.053 s^{-1}, leading to a significant

loss of oxidised mediator within tens of seconds [156]. This chemical decay introduces scan-rate-dependent hysteresis, progressive current loss and time-dependent shifts in apparent formal potential, even when the electron-transfer step itself is fast.

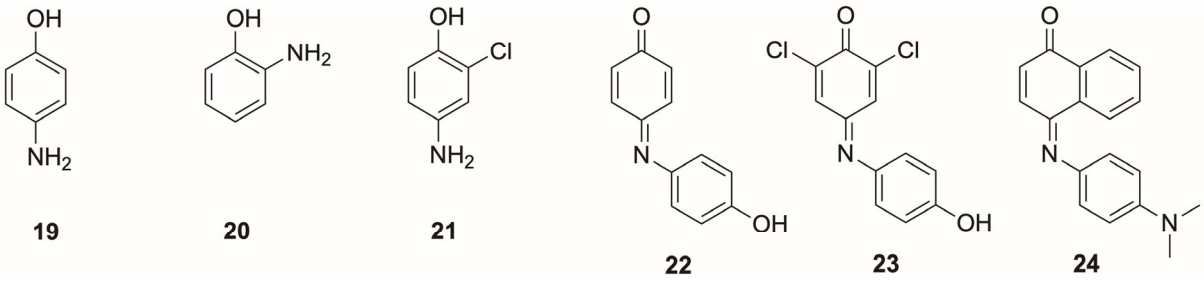
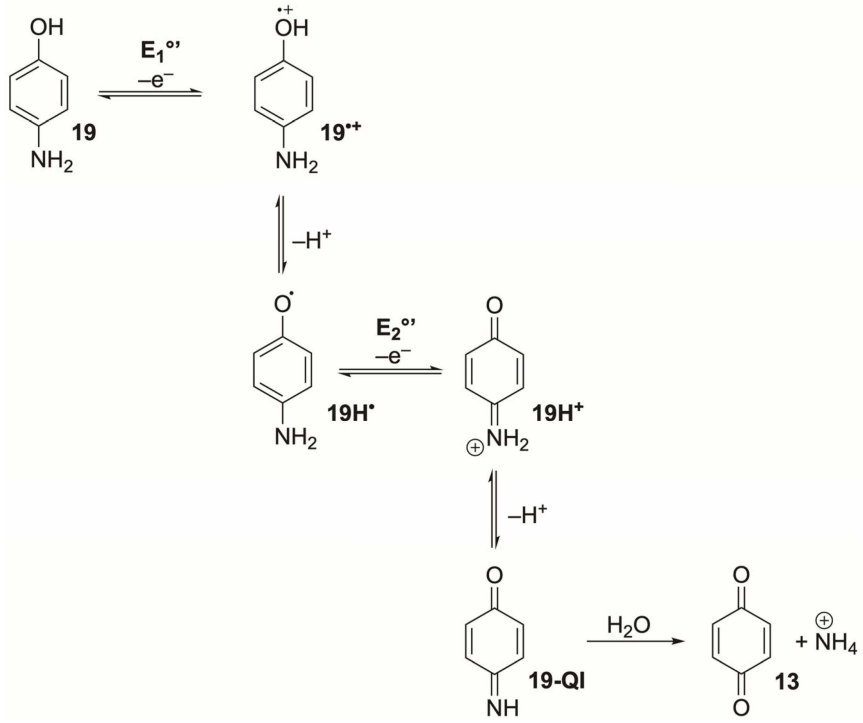


Figure 5. Representative structures of aminophenol and indophenol mediators. (**19**) p-aminophenol, (**20**) o-aminophenol, (**21**) 4-amino-2-chlorophenol, (**22**) phenolindophenol, (**23**) indophenol blue, and (**24**) 2,6-dichlorophenolindophenol.



Scheme 4. Electrochemical oxidation mechanism of p-aminophenol (**19**) in aqueous media. Horizontal steps denote ET, and vertical steps denote proton transfer, except for the last step, which represents an irreversible chemical reaction with water to yield **13**.

Interfacial chemistry further amplifies irreversibility. Adsorption and radical coupling promote fouling during **19** turnover. At the same time, the o- and m-isomers undergo rapid polymerisation, further reducing apparent reversibility [152,157,158]. Confinement within self-assembled monolayers or polymer matrices can narrow ΔE_p and suppress mediator loss, but this reflects restricted chemical pathways rather than genuine thermodynamic reversibility [155,159]. Thus, aminophenols function as electrochemically fast but chemically unstable mediators, whose operational reversibility is governed by the microenvironment, timescale, and the kinetics of **19-QI** decay rather than by intrinsic electron-transfer behaviour.

Despite these mechanistic liabilities, aminophenols remain highly effective enzyme reporters. Compared with classical phenolic reporters, the p-aminophenol family of reporters

operates at lower potentials, reduces fouling on carbon electrodes, improves selectivity against common interferents and offers strong optical signatures. These advantages extend to DNA and protein hybridisation assays and to redox cycling schemes in which chemical reductants such as hydrazine regenerate **19** from its quinone-imine [160–163], allowing low-background, single-electrode amplification.

These mechanistic features underpin the broad use of aminophenols in biosensing formats, including alkaline phosphatase and esterase assays using p-aminophenol phosphate or acyl-protected aminophenols, HRP-driven ELISAs based on the controlled generation of **19**, and nucleic-acid sensors that exploit hydrazine-mediated redox cycling of **19** for signal amplification [160,164–166].

Indophenols occupy a neighbouring but mechanistically distinct region of the high-potential domain. Phenolindophenol and related dyes (**22**–**24**) behave as reversible $2e^-/2H^+$ PCET couples, closely paralleling quinone/hydroquinone chemistry rather than the ECEC pathways of aminophenols. Their redox interconversion occurs with $E^{\circ\prime}$ between 0.00 and 0.10 V vs. Ag/AgCl and displays a characteristic pH-dependent shift consistent with PCET [147,167]. Immobilised indophenols function as efficient oxidising mediators in FAD-GDH bioanodes, where they establish catalytic onset potentials around 0.05–0.10 V and relay electrons through polydopamine or metal-oxide films [147]. Their reversible redox behaviour also supports NADH oxidation on graphite, zirconium phosphate and other inorganic supports, enabling low-overpotential dehydrogenase sensors and biofuel cell anodes [167]. Unlike aminophenols, indophenols do not undergo rapid polymerisation, though extended electrochemical cycling can generate reactive oxygen species and gradually degrade mediator stability [167].

Although indophenols display clean, symmetric voltammetric waves, their electrochemical behaviour is best classified as high quasi-reversible rather than fully reversible. The oxidised/leuco interconversion proceeds through a $2e^-/2H^+$ proton-coupled mechanism. Still, the observed peak separations on carbon electrodes, typically ΔE_p~55–70 mV, are significantly larger than the ~30 mV expected for a truly reversible $2e^-$ couple [157,168,169]. These ΔE_p values instead reflect a collapsed two-step process that behaves like a fast but not fully reversible $1e^-$ wave, consistent with rapid PCET and semiquinone equilibration without attainment of strict Nernstian conditions. The modest scan-rate dependence and near-unity i_{pa}/i_{pc} ratios confirm rapid heterogeneous ET. In contrast, the well-defined pH dependence of $E^{\circ\prime}$ (-59 to -67 mV pH^{-1}) supports a tightly coupled $2H^+/2e^-$ mechanism [169]. Importantly, the leuco form is chemically stable on voltammetric timescales, and adsorption is weak, allowing indophenols to maintain operational quasi-reversibility even in immobilised films. Deviations from ideality arise primarily from slow autoxidation or photodegradation rather than intrinsic kinetic limitations [168]. Thus, indophenols occupy a category distinct from aminophenols: chemically robust and electrochemically fast, yet still formally quasi-reversible rather than fully reversible $2e^-$ mediators.

In practical biosensor architectures, these two families illustrate contrasting design constraints. Aminophenols, whether operating near 0.1–0.3 V or, in N-acylated forms, around 0.55–0.60 V, require careful control of applied bias, spatial confinement within matrices, controlled pH and short measurement windows to suppress hydrolysis and radical coupling. Indophenols, although restricted to a narrower PCET window, exhibit markedly greater chemical reversibility. Together, they define the high-potential edge of the organic mediator space, bridging towards metal-complex mediators while providing chromogenic, spectroelectrochemical and film-forming attributes that can be exploited or rigorously suppressed, depending on the intended biosensor function.

3.5. Azines, Phenothiazines and Phenoxazines

Azines, phenothiazines and phenoxazines (Figure 6) form a unified class of aromatic dyes whose redox chemistry is governed by heteroatom-stabilised cationic or quasi-quinonoid frameworks. Their formal potentials cluster between −0.05 and 0.15 V vs. Ag/AgCl for most dialkyl- and diaryl-substituted systems, with pronounced pH-dependence arising from protonation equilibria at ring nitrogens and phenolic or heteroatom sites [170–176]. Unlike aminophenols, whose oxidised quinone-imines are chemically fragile, these dyes typically undergo fast, chemically robust proton-coupled electron-transfer processes in aqueous media. In most cases, two rapid one-electron/proton-transfer events (an ECEC sequence) occur at closely spaced potentials, so that the voltammetric response appears as a single $2e^-$ envelope with high quasi-reversibility rather than as two fully resolved $1e^-$ couples. Phenothiazines (**27**–**29**) and phenoxazines (**30**–**32**) stabilise their oxidised states through extended N-S or N-O heteroaromatic delocalisation, exhibit low reorganisation energies and yield symmetrical, chemically stable voltammetric waves on carbon, gold and metal-oxide electrodes [170–176]. Collectively, their structural rigidity, chemical resilience and predictable proton/electron-transfer behaviour underpin their reliability as mediators across a wide range of biosensing architectures.

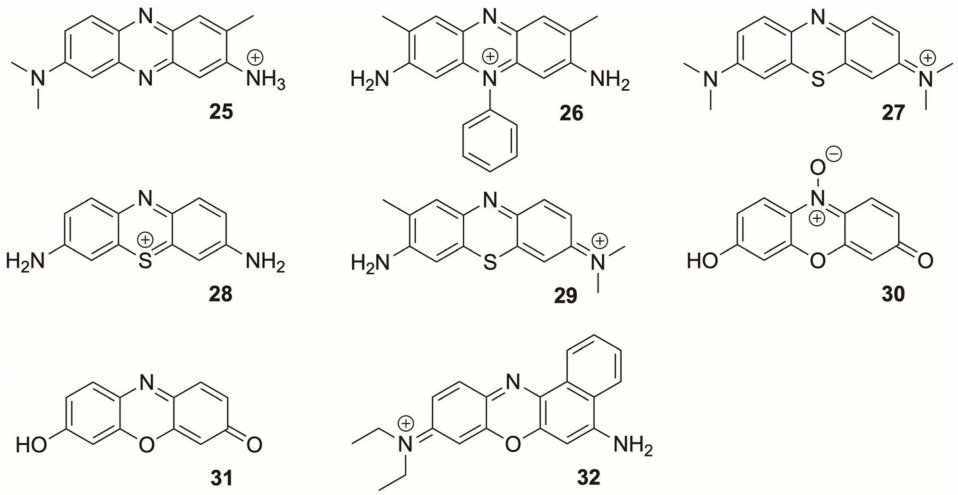


Figure 6. Representative structures of azine, phenothiazine and phenoxazine mediators. Neutral Red (**25**) and Safranine O (**26**) illustrate diazinium-centred azines; Methylene Blue (**27**), Thionine (**28**) and Toluidine Blue O (**29**) represent phenothiazinium dyes; Resazurin (**30**), Resorufin (**31**) and Nile Blue A (**32**) depict phenoxazine mediators.

Within this family, phenothiazines, exemplified by **27**, **28** and their N-alkylated analogues, undergo a fast, quasi-reversible $2e^-/2H^+$ transformation between the phenothiazinium cation and its leuco form. Although this can resemble a concerted $2e^-$ PCET couple, kinetic analysis and ΔE_p values of 55–70 mV indicate that the overall response reflects two rapid, sequential ECEC steps whose individual electron–proton transfers collapse into a single voltammetric wave rather than an ideal Nernstian $2e^-$ process [21,177,178]. Classic surface studies show that the oxidised phenothiazinium cation is reduced rapidly and chemically reversibly, giving small peak separations and surface-controlled kinetics [21]. Adsorption on carbon is strong, with monolayer-level coverages, fast heterogeneous ET and modest potential shifts associated with π-π ordering and partial immobilisation [178]. These properties underpin their widespread use in NADH-oxidising electrodes and peroxidase-based bioelectrocatalysis. Electropolymerised phenothiazine films, including poly(**27**) and poly(**28**), form stable, conductive layers with well-defined formal potentials that depend on polymer microsite acidity and counter-ion composition, and they show enhanced oper-

ational stability relative to the monomeric dyes [177,178]. Methylene Blue, in particular, sits near 0.00–0.05 V vs. Ag/AgCl at neutral pH, enabling low-overpotential oxidation of reduced cofactors and efficient wiring of peroxidases and dehydrogenases in both solution and immobilised formats [179,180].

Azines share many of these electrochemical signatures but use diazinium-centred PCET rather than S/N-stabilised redox centres. Neutral Red (**25**), Safranine O (**26**), and related mono- or disubstituted azines display quasi-reversible $2e^-/2H^+$ transformations with formal potentials set by the protonation state of the ring nitrogens [175,176]. Their surface behaviour is dominated by strong π-stacking and partial orientational ordering on carbon, giving Nernstian surface waves at low coverage and mixed diffusion–adsorption kinetics at higher loadings [175,176]. In biosensing formats, azines support electrocatalytic NADH oxidation at modest overpotentials and can be entrapped in polymer, silica or oxide matrices to form low-drift mediator layers [176,181]. Their redox stability over several pH units, combined with high molar absorptivity, also enables dual electrochemical-optical readout in dehydrogenase and DNA-hybridisation platforms [179].

Phenoxazines occupy the most delocalised end of this class and often exhibit the cleanest high-quasi-reversible, quinone-like PCET behaviour. Resazurin (**30**) and resorufin (**31**) provide canonical examples: voltammetry reveals a two-step $2e^-$ sequence with closely aligned waves and strong pH dependence, consistent with proton-coupled interconversion of semiquinonoid intermediates [172–174]. Although their ΔE_p values (~55–70 mV) exceed the 30 mV criterion for a fully reversible $2e^-$ couple, the rapid establishment of PCET equilibria and negligible build-up of intermediates allow them to behave operationally reversible on analytical timescales. Electropolymerisation yields conductive poly(**32**) and related poly(oxazine) films with densely accessible redox sites and high apparent ET rates, exploited for NADH detection and oxidase-based sensing [182]. Structural tunability also permits covalent wiring: β-(10-phenoxazinyl)propionic acid can be conjugated to GOx, generating a wired enzyme with a stable quasi-reversible $2e^-$ mediator couple around 0.42 V vs. Ag/AgCl that supports catalytic glucose oxidation via combined intra- and intermolecular ET pathways [183].

Across azines, phenothiazines and phenoxazines, several unifying mechanistic principles emerge. First, unlike aminophenols, their oxidised forms do not undergo rapid hydrolysis, rearrangement or polymer-initiated side reactions, so they maintain high quasi-reversible voltammetry over the timescales relevant to biosensing. Second, their potential–pH profiles are dominated by proton-coupled ET, with slopes of ~55–70 mV pH^{-1} that are characteristic of fast, stepwise PCET [173,174]. Third, immobilised or electropolymerised variants exhibit enhanced chemical and operational stability, suppressed mediator leaching and high apparent ET rates mediated through surface-confined states or redox-polymer hopping, enabling low-overpotential operation with improved cycling stability and reduced signal drift [177,180,182]. Finally, their combination of intense optical transitions, rigid heteroaromatic frameworks and rapid, quasi-reversible ET allow these dyes to act simultaneously as mediators, redox-polymer scaffolds and electrochemical-spectroscopic reporters, making them among the most versatile mediator families in the medium-potential region of the organic window.

4. Mediator Potential Landscape and Design Constraints

The formal potentials compiled in Figure 7 outline the electrochemical landscape spanned by the mediator families discussed in this review. Figure 7 is intended as a comparative framework rather than a performance ranking, illustrating how mediator class and coordination environment define the practically accessible potential window for reversible biosensor operation. A common reference scale highlights where electron-transfer

thermodynamics are favourable, but these windows alone do not guarantee operational reversibility [3,23]. Chemical stability of the oxidised and reduced states, shaped by proton activity, microenvironment, nucleophilicity and intrinsic reactivity, is an equally decisive constraint. Thus, a mediator may fall well within its nominal potential band yet still lose reversibility through parallel chemistry, as exemplified by aminophenols whose quinone-imine forms rapidly hydrate and rearrange irrespective of applied bias [3,7,12]. Accordingly, the shaded ranges in Figure 7 indicate where electrochemical reversibility can, in principle, be achieved, while the true recoverability of a redox couple ultimately depends on the chemical robustness of each oxidation state under operating conditions [18,23].

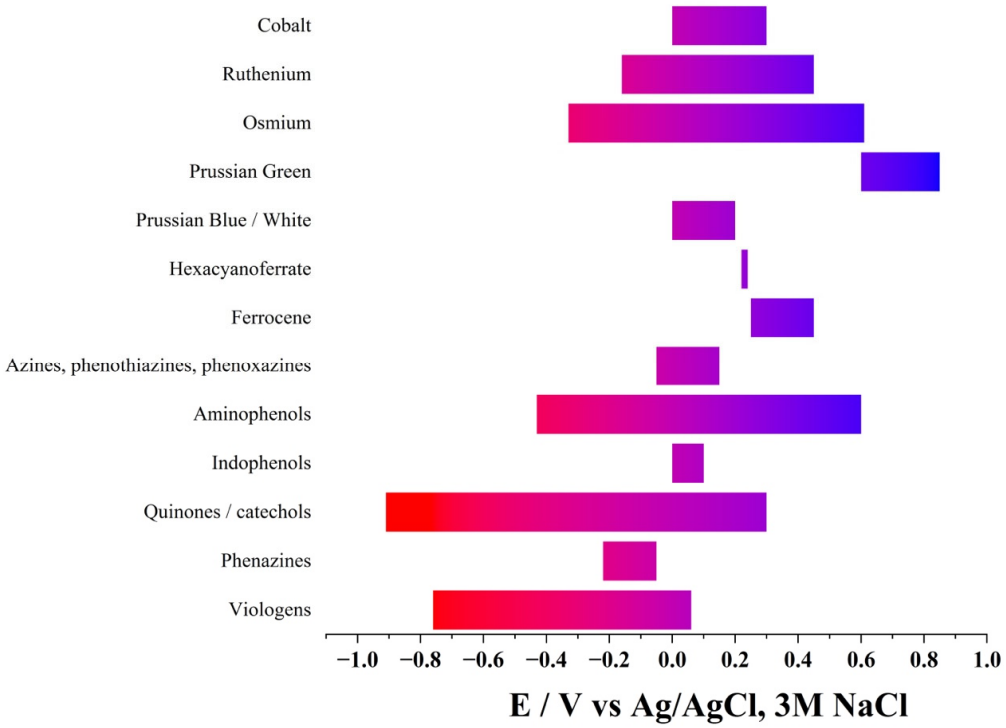


Figure 7. Formal potential ranges of major mediator families discussed in this review, expressed versus Ag AgCl, 3 M NaCl.

At the most negative end, viologens and extended anthraquinone derivatives occupy approximately −0.90 to −0.20 V vs. Ag/AgCl. These low potentials minimise overlap with endogenous oxidants and couple well to low-potential enzymatic cofactors. Their advantage is tempered by narrow stability limits: viologen radicals dimerise, disproportionate, bind surfaces and decay rapidly under aerobic conditions, while anthraquinones undergo pH-dependent autoxidation, hydration and Michael-type reactivity. Their position at the bottom of the scale, therefore, represents both valuable low-bias access and the chemical penalties of strongly reducing states.

Progressing toward more positive potentials, phenazines, indophenols, aminophenols, phenoxazines and related dye systems populate roughly −0.22 to 0.38 V. Phenazines can function as relatively clean two-electron mediators, but most dye families in this region are governed by proton-coupled pathways and extensive side chemistry. Aminophenols illustrate this sharply: their initial oxidation triggers an ECEC sequence that generates quinone-imines, which hydrolyse or polymerise rapidly, precluding genuine reversibility even when voltammograms appear superficially stable. Indophenols and phenoxazines display better apparent reversibility but remain strongly influenced by pH, proton inventory and hydrogen bonding. Collectively, this region represents a mechanistic transition zone where attractive potentials coexist with growing constraints on redox cycling.

Quinones and catechols span a broad window from strongly negative potentials to roughly 0.2–0.3 V at neutral pH. Although their two-electron/two-proton couples are, in principle, quasi-reversible, the oxidised quinone states are short-lived in aqueous media. Hydration, nucleophilic attack, semiquinone generation and polymerisation directly compete with electrode-driven cycling. The apparent breadth of the quinone potential band, therefore, does not translate into broad practical mediator utility: long-term reversibility is limited to narrow pH and microenvironmental regimes or to single-use sensing architectures.

Between 0.0 and ca. 0.30 V lie cobalt macrocycles, hexacyanoferrate species and PB, each governed by distinct mechanistic constraints. Cobalt macrocycles undergo inner-sphere Co^{2+}/Co^{3+} transitions that approach the oxidation potentials of common interferents, narrowing their safe anodic window. Hexacyanoferrate is formally an outer-sphere complex, yet can deviate from ideal Nernstian behaviour on practical electrodes due to ion pairing, adsorption, and interactions with underlying metal surfaces. Prussian Blue enables exceptionally low-bias peroxide detection, but its cyanide-bridged lattice becomes progressively unstable under neutral to alkaline conditions and degrades upon repeated redox cycling, limiting long-term operation near physiological pH.

Beyond 0.30 V, the window becomes progressively constrained by the oxidation of ascorbate, urate, phenolics and other matrix components. Nonetheless, this region contains the most tuneable mediator families: ruthenium and osmium polypyridyl complexes. Osmium derivatives span nearly a volt (−0.33 to 0.61 V), with ruthenium analogues covering −0.16 to 0.45 V. Their outer-sphere kinetics, ligand tunability, and compatibility with redox polymers enable precise matching to enzymatic cofactors. However, their higher operating potentials increase susceptibility to ligand exchange and photochemical and redox-induced processes that progressively shift mediator behaviour, as well as to parasitic oxidation, necessitating immobilisation strategies to prevent leaching. Combined with the high cost of Ru and Os, these factors define the practical upper limit of their suitability for disposable or resource-limited platforms.

At the extreme upper boundary, the PB to PG transition (ca. 0.60 to 0.85 V) exemplifies where mediator behaviour fails outright. The oxidised PG state is chemically unstable, undergoing lattice contraction, vacancy formation and irreversible loss of electroactivity. It represents a redox transition that is electrochemically accessible yet chemically unrecoverable, and therefore incompatible with mediator function.

Across all mediator families, Figure 7 shows that reversibility is shaped as much by stability, pH-dependent equilibria, microstructure and coordination environment as by intrinsic redox potential. Instabilities at both ends of the scale define its boundaries, while systems near the centre highlight how narrow the operational space becomes when fast electron transfer and long-term chemical durability must coexist in complex matrices. These constraints ultimately determine which mediator families support robust biosensing architectures and which remain limited to niche, single-use or predominantly catalytic roles.

These design constraints become most apparent under continuous operation and in complex sample matrices, where mediator stability, drift and fouling ultimately determine practical sensor lifetime.

Practical Performance of Redox Mediators Under Continuous and Complex Sensing Conditions

While formal potential windows and electron-transfer kinetics define whether a mediator is thermodynamically viable, practical biosensing performance is ultimately governed by stability, drift, fouling susceptibility and tolerance to complex sample matrices. These factors become especially critical under continuous or long-term operation, where even modest chemical or interfacial degradation accumulates into significant signal loss [23,184].

Quantitative reporting of such parameters remains inconsistent across the literature, limiting direct comparison between mediator classes [3]. Nevertheless, several representative trends emerge. Within the continuous biosensing literature, wired enzyme systems based on osmium redox polymers provide the clearest benchmarks for long-term operation. Early continuous glucose sensing studies demonstrated stable amperometric responses over many hours, with gradual sensitivity loss attributed primarily to surface fouling or local microenvironmental changes rather than degradation of electron-transfer capability [185]. Cross-linked osmium polymer hydrogels further improved operational lifetimes, extending the time required for signal decay to 50% from tens of hours to approximately one hundred hours under continuous turnover, while comparable ruthenium polymers exhibited substantially shorter operational lifetimes under identical conditions [186]. These results highlight that reversibility alone is insufficient; chemical robustness of the oxidised and reduced states under sustained cycling is equally decisive.

Small-molecule mediators exhibit more variable long-term behaviour. Ferrocene and ferrocene-derived redox polymers can display prolonged cycling with low baseline drift when immobilised in well-designed polymer matrices, but performance is strongly dependent on film architecture and protection from protein adsorption [54,187]. In contrast, quinones and phenazines, despite often exhibiting near-Nernstian behaviour in short-term electrochemical characterisation, are prone to side reactions such as hydration, nucleophilic addition or dimerisation under extended operation. These processes progressively diminish reversibility and promote electrode passivation, leading to signal drift even when formal potentials remain within the desired operating window [188,189].

Fouling and matrix effects further differentiate mediator classes in practical settings. Protein adsorption and biofouling are dominant failure modes in serum and whole-blood measurements, particularly for mediators operating at relatively positive potentials [56,184]. Studies employing permselective membranes, polymer tethering or redox polymer encapsulation demonstrate that effective isolation of the mediator from the bulk matrix can substantially reduce drift, with reports of stable amperometric responses over one hour or longer in protein-containing media accompanied by signal losses below 15% [55,188]. Inorganic mediator films such as PB and hexacyanoferrates offer additional advantages for continuous monitoring due to their low operating potentials, which suppress parasitic reactions and reduce fouling, enabling extended stable operation in peroxide-based biosensing schemes [43,190,191].

Overall, available data indicate that mediator performance under practical biosensing conditions cannot be inferred solely from formal potential or short-term reversibility. Long-term stability is maximised when reversible electron transfer is coupled with chemical inertness of intermediate redox states, low susceptibility to side reactions, and effective isolation from complex matrices [3,23]. These considerations reinforce reversibility as a necessary but not sufficient design criterion, and emphasise the importance of integrating electrochemical, chemical and interfacial stability in mediator selection for continuous and real-world biosensing applications.

5. Conclusions and Future Perspectives

Reversibility remains the defining criterion that distinguishes functional redox mediators from species that are merely redox-active. Across the mediator classes examined here, reversible behaviour arises most reliably from coordination and organometallic frameworks, where ligand-field control, rigid coordination geometries and outer-sphere electron-transfer pathways stabilise both oxidation states and minimise structural or chemical reorganisation during cycling. This stands in contrast to many organic mediator families, such as quinones, phenazines, indophenols and aminophenols, which offer broad tunability but

whose oxidised or reduced states are intrinsically constrained by proton-coupled equilibria, hydration pathways and polymerisation reactions that erode long-term cycling stability.

The potential landscape shows that no mediator family is universally optimal; instead, the chemically recoverable redox couples with the broadest operational windows and the greatest structural tunability arises predominantly from metal-ligand architectures. Ferrocene derivatives provide highly modular mid-potential couples; cobalt macrocycles introduce finely tuneable inner-sphere Co^{2+}/Co^{3+} chemistry and PCET control within a mid-potential domain that overlaps organic dyes; and ruthenium and osmium polypyridyl complexes span nearly a full volt with low reorganisation energies and exceptional outer-sphere kinetics. Their limitations, which include chiefly cost, immobilisation requirements and aqueous-stability considerations, define practical rather than mechanistic boundaries. In contrast, organic systems, while valuable for single-use or low-bias sensing, often face fundamental chemical limitations that limit long-term cycling.

Future progress, therefore, depends on leveraging inorganic design principles to stabilise redox states and control microenvironmental reactivity. Three avenues appear particularly promising: First, polymer-confined or tethered metal-ligand architectures can protect redox centres from hydration and nucleophilic attack while maintaining rapid electron hopping. Second, hybrid organic-inorganic mediator platforms may enable decoupling of potential tuning from chemical instability, pairing coordination robustness with organic electronic flexibility. Third, computationally guided mediator design, integrating Marcus theory with ligand-field modelling and microenvironment simulations, offers a route to predicting conditions under which nominally irreversible systems may be rendered quasi-reversible through confinement or controlled proton inventories.

In parallel, recent advances in sensing platforms increasingly shift the relevance of mediator reversibility from a purely electrochemical consideration to a systems-level constraint. Nanocomposite-modified electrodes incorporating carbon nanomaterials, metal oxides or hybrid conductive networks offer opportunities to stabilise mediator environments by improving charge delocalisation, suppressing local concentration gradients and physically restricting deleterious side reactions. In such architectures, reversible mediators are particularly advantageous, as their redox cycling can be sustained within confined or heterogeneous domains without cumulative chemical degradation. Similarly, the emergence of flexible and wearable electrochemical sensors places new demands on mediator robustness, as repeated mechanical deformation, variable hydration and long-term operation amplify the consequences of even minor irreversible processes. Under these conditions, mediators that maintain chemical stability across repeated redox cycles are better suited for integration into redox polymers, stretch-tolerant matrices and printed conductive films. Finally, scalable fabrication approaches such as screen printing and additive manufacturing further emphasise the importance of reversible mediators that tolerate drying–rehydration cycles, prolonged storage and repeated operation without loss of electrochemical fidelity. Collectively, these developments suggest that reversibility is becoming an increasingly enabling property for emerging sensing technologies, rather than merely a desirable electrochemical attribute.

Despite extensive study, several unresolved issues continue to complicate the interpretation and comparison of mediator reversibility across the biosensing literature. Most notably, electrochemical reversibility inferred from short-term voltammetric criteria is frequently conflated with chemical recoverability under sustained operation, even though these concepts are not equivalent. Apparent near-Nernstian behaviour may persist in systems that undergo slow but cumulative chemical degradation, particularly for proton-coupled or EC-type mediators. In addition, the metrics used to assess reversibility remain inconsistent, with parameters such as peak separation, heterogeneous rate constants or cat-

alytic current retention often reported in isolation, while long-term stability, baseline drift and cumulative cycling damage are rarely quantified in a standardised manner. These ambiguities are further amplified by strong platform dependence, as immobilisation strategy, microenvironment and matrix composition can dominate mediator behaviour. They are further compounded by the frequent reliance on characterisation in buffered electrolytes, with mediator performance often implicitly extrapolated to complex biological matrices such as blood, plasma or milk without systematic validation under realistic conditions. Addressing these unresolved issues will require clearer operational definitions of reversibility, broader adoption of time-resolved performance metrics and more explicit separation of intrinsic mediator chemistry from interfacial and matrix effects.

Finally, mediator suitability is inherently time-scale dependent. Organic mediators may perform well in short-duration or single-use assays, yet their oxidised states often accumulate damage under continuous operation. In contrast, metal-centred systems support extended cycling but impose cost and synthetic complexity that must align with intended deployment formats. Achieving this alignment requires shifting from empirical mediator selection to a mechanistically grounded design, with reversibility, as shaped by coordination chemistry, ligand architecture and the microenvironment, serving as the central organising principle.

Funding: This research received no external funding.

Data Availability Statement: Not applicable.

Conflicts of Interest: The author declares no conflicts of interest.

Abbreviations

The following abbreviations are used in this manuscript:

BOx	bilirubin oxidase
bpy	2,2′-bipyridine
CV	cyclic voltammetry
dmabpy	4-dimethylamino-2,2′-bipyridine
dmbpy	4,4′-dimethyl-2,2′-bipyridine
dmObpy	4,4′-dimethoxy-2,2′-bipyridine
EC	electron transfer followed by a chemical step
EC′	electron-transfer/chemical catalytic regeneration mechanism
ECEC	electron-transfer/chemical/electron-transfer/chemical sequence
ET	electron transfer
FAD	flavin adenine dinucleotide
Fc	ferrocene
GDH	glucose dehydrogenase
GOx	glucose oxidase
HRP	horseradish peroxidase
k°	standard heterogeneous electron-transfer rate constant
MOPS	3-(N-morpholino)propanesulfonic acid (Good's buffer)
NAD	nicotinamide adenine dinucleotide
NHE	normal hydrogen electrode
PB	Prussian Blue
PBS	phosphate-buffered saline
PCET	proton-coupled electron transfer
PG	Prussian Green
phen	1,10-Phenanthroline
phendione	1,10-Phenanthroline-5,6-dione

phpy	phenylpyridine (cyclometalating C–N ligand)
POM	Polyoxometalate
Poly(Vim)	poly(vinylimidazole)
poly(Vpy)	poly(vinylpyridine)
Poly(Vpyr-co-aa)	poly(N-vinylpyrrolidone-co-acrylic acid)
PQQ	pyrroloquinoline quinone
PW	Prussian White
SAM	self-assembled monolayer
topy	*p*-Tolylpyridine ligand

References

1. Sadana, A. *Engineering Biosensors: Kinetics and Design Applications*; Academic Press (Elsevier): San Diego, CA, USA, 2002.
2. Zhang, X.; Huangxian, J.; Wang, J. *Electrochemical Sensors, Biosensors and Their Biomedical Applications*; Academic Press: Amsterdam, The Netherlands, 2008.
3. Campuzano, S.; Pedrero, M.; Gamella, M.; Serafín, V.; Yáñez-Sedeño, P.; Pingarrón, J.M. Beyond Sensitive and Selective Electrochemical Biosensors: Towards Continuous, Real-Time, Antibiofouling and Calibration-Free Devices. *Sensors* **2020**, *20*, 3376. [CrossRef]
4. Bollella, P.; Katz, E. Enzyme-Based Biosensors: Tackling Electron Transfer Issues. *Sensors* **2020**, *20*, 3517. [CrossRef]
5. Savéant, J.-M. *Elements of Molecular and Biomolecular Electrochemistry: An Electrochemical Approach to Electron Transfer Chemistry*; John Wiley & Sons, Inc.: Hoboken, NJ, USA, 2006.
6. Lee, H.; Reginald, S.S.; Sravan, J.S.; Lee, M.; Chang, I.S. Advanced strategies for enzyme–electrode interfacing in bioelectrocatalytic systems. *Trends Biotechnol.* **2025**, *43*, 1328–1355. [CrossRef]
7. Xiao, X.; Yan, X.; Magner, E.; Ulstrup, J. Polymer coating for improved redox-polymer-mediated enzyme electrodes: A mini-review. *Electrochem. Commun.* **2021**, *124*, 106931. [CrossRef]
8. Yang, T.; Liu, J.; Wang, Y.; Li, X.; Zhang, Y.; Huang, Q.; Ge, Y.; Tian, R.; Pu, Y.; He, Q.; et al. Rational design and development of phenazine-based electron mediators for enzyme-based biosensors: Advancing clinical diagnostics through computational exploration. *Sens. Actuators B Chem.* **2025**, *426*, 137059. [CrossRef]
9. Zhang, H.; Cheng, M.; Li, Y.; Chen, W. Quinoid Redox Mediators and Their Involvement in Environmental Pollution Treatment. *Water* **2023**, *15*, 3981. [CrossRef]
10. Demkiv, O.; Gayda, G.; Stasyuk, N.; Brahinetz, O.; Gonchar, M.; Nisnevitch, M. Nanomaterials as Redox Mediators in Laccase-Based Amperometric Biosensors for Catechol Assay. *Biosensors* **2022**, *12*, 741. [CrossRef]
11. Gu, Y.; Yuan, L.; Jia, L.; Xue, P.; Yao, H. Recent developments of a co-immobilized laccase–mediator system: A review. *RSC Adv.* **2021**, *11*, 29498–29506. [CrossRef] [PubMed]
12. Dhand, C.; Das, M.; Datta, M.; Malhotra, B.D. Recent advances in polyaniline based biosensors. *Biosens. Bioelectron.* **2011**, *26*, 2811–2821. [CrossRef] [PubMed]
13. Shoaie, N.; Daneshpour, M.; Azimzadeh, M.; Mahshid, S.; Khoshfetrat, S.M.; Jahanpeyma, F.; Gholaminejad, A.; Omidfar, K.; Foruzandeh, M. Electrochemical sensors and biosensors based on the use of polyaniline and its nanocomposites: A review on recent advances. *Microchim. Acta* **2019**, *186*, 465. [CrossRef] [PubMed]
14. Saleem, M.; Yu, H.; Wang, L.; Zain-ul-Abdin; Khalid, H.; Akram, M.; Abbasi, N.M.; Huang, J. Review on synthesis of ferrocene-based redox polymers and derivatives and their application in glucose sensing. *Anal. Chim. Acta* **2015**, *876*, 9–25. [CrossRef]
15. Veríssimo, M.I.S.; Evtuguin, D.V.; Gomes, M.T.S.R. Polyoxometalate Functionalized Sensors: A Review. *Front. Chem.* **2022**, *10*, 2022. [CrossRef]
16. Lu, C.; Tang, Z.; Wang, D.; Chen, L.; Zhao, J. Advances in polyoxometalate-based electrochemical sensors in the last three years. *Anal. Methods* **2024**, *16*, 5133–5145. [CrossRef]
17. Li, J.; Tang, Z.; Chen, L.; Zhao, J. Recent research progress in polyoxometalate-based composite materials applied to electrochemical biosensors for biomolecule detection. *Nanoscale* **2025**, *17*, 21379–21399. [CrossRef]
18. Bard, A.J.; Faulkner, L.R. *Electrochemical Methods: Fundamentals and Applications*; Wiley: New York, NY, USA, 2001.
19. Matsuda, H.; Ayabe, Y. On the theory of Randles–Ševčík cathodic polarography. *Z. Elektrochem. Ber. Bunsenges. Phys. Chem.* **1955**, *59*, 494–503. [CrossRef]
20. Torriero, A.A.J. Characterization of decamethylferrocene and ferrocene in ionic liquids: Argon and vacuum effect on their electrochemical properties. *Electrochim. Acta* **2014**, *137*, 235–244. [CrossRef]
21. Laviron, E. General expression of the linear potential sweep voltammogram in the case of diffusionless electrochemical systems. *J. Electroanal. Chem. Interfacial Electrochem.* **1979**, *101*, 19–28. [CrossRef]

22. Tsujimura, S. Developments in Bioelectrocatalysis Using Rationally Designed Enzyme Electrode Materials. *Electrochemistry* **2024**, *92*, 101002. [CrossRef]
23. Heller, A.; Feldman, B. Electrochemical glucose sensors and their applications in diabetes management. *Chem. Rev.* **2008**, *108*, 2482–2505. [CrossRef] [PubMed]
24. Karyakin, A.A.; Karyakina, E.E. Prussian Blue-based 'artificial peroxidase' as a transducer for hydrogen peroxide detection. Application to biosensors. *Sens. Actuators B Chem.* **1999**, *57*, 268–273. [CrossRef]
25. VandeZande, G.R.; Olvany, J.M.; Rutherford, J.L.; Rasmussen, M. Enzyme Immobilization and Mediation with Osmium Redox Polymers. In *Enzyme Stabilization and Immobilization: Methods and Protocols*; Minteer, S.D., Ed.; Springer: New York, NY, USA, 2017; pp. 165–179.
26. Torriero, A.A.J. Reference systems for voltammetric measurements in ionic liquids. In *Electrochemistry in Ionic Liquids. Volume 1: Fundamentals*; Torriero, A.A.J., Ed.; Springer: Cham, Switzerland, 2015; Volume 1.
27. Dong, L.; Zeng, X.; Xiong, Y.; Xiao, X.; Zhan, D.; Wang, S. Enzymatic bioelectrodes based on ferrocene-modified metal-organic layers for electrochemical glucose detection. *Anal. Bioanal. Chem.* **2025**, *417*, 2217–2224. [CrossRef]
28. Neumann, B.; Wollenberger, U. Electrochemical Biosensors Employing Natural and Artificial Heme Peroxidases on Semiconductors. *Sensors* **2020**, *20*, 3692. [CrossRef] [PubMed]
29. Eckermann, A.L.; Feld, D.J.; Shaw, J.A.; Meade, T.J. Electrochemistry of redox-active self-assembled monolayers. *Coord. Chem. Rev.* **2010**, *254*, 1769–1802. [CrossRef]
30. Chidsey, C.E.D. Free Energy and Temperature Dependence of Electron Transfer at the Metal-Electrolyte Interface. *Science* **1991**, *251*, 919–922. [CrossRef]
31. Koide, S.; Yokoyama, K. Electrochemical characterization of an enzyme electrode based on a ferrocene-containing redox polymer. *J. Electroanal. Chem.* **1999**, *468*, 193–201. [CrossRef]
32. Crulhas, B.R.; Ramos, N.P.; Basso, C.R.; Costa, V.E.; Castro, G.R.; Pedrosa, V.A. Fabrication and characterization of ferrocenece containing hydrogel for glucose biosensor application. *Int. J. Electrochem. Sci.* **2014**, *9*, 7596–7604. [CrossRef]
33. Estrada-Osorio, D.V.; Escalona-Villalpando, R.A.; Gutiérrez, A.; Arriaga, L.G.; Ledesma-García, J. Poly-L-lysine-modified with ferrocene to obtain a redox polymer for mediated glucose biosensor application. *Bioelectrochemistry* **2022**, *146*, 108147. [CrossRef] [PubMed]
34. Torriero, A.A.J.; Mruthunjaya, A.K.V. Ferrocene-Based Electrochemical Sensors for Cations. *Inorganics* **2023**, *11*, 472. [CrossRef]
35. Alonso, B.; Armada, P.G.A.; Losada, J.; Cuadrado, I.; González, B.; Casado, C.M. Amperometric enzyme electrodes for aerobic and anaerobic glucose monitoring prepared by glucose oxidase immobilized in mixed ferrocene–cobaltocenium dendrimers. *Biosens. Bioelectron.* **2004**, *19*, 1617–1625. [CrossRef] [PubMed]
36. Al-Sagur, H.; Shanmuga sundaram, K.; Kaya, E.N.; Durmuş, M.; Basova, T.V.; Hassan, A. Amperometric glucose biosensing performance of a novel graphene nanoplatelets-iron phthalocyanine incorporated conducting hydrogel. *Biosens. Bioelectron.* **2019**, *139*, 111323. [CrossRef]
37. Heller, A. Redox hydrogel-based electrochemical biosensors. In *Biosensors: A Practical Approach*; Cooper, J.M., Cass, A.E.G., Eds.; Oxford Academic: Oxford, UK, 2004; Volume 2.
38. Fernández, L.; Alvarez-Paguay, J.; González, G.; Uribe, R.; Bolaños-Mendez, D.; Piñeiros, J.L.; Celi, L.; Espinoza-Montero, P.J. Electrochemical Sensor for Hydrogen Peroxide Based on Prussian Blue Electrochemically Deposited at the TiO_2-ZrO_2–Doped Carbon Nanotube Glassy Carbon-Modified Electrode. *Front. Chem.* **2022**, *10*, 2022. [CrossRef]
39. Gayda, G.Z.; Demkiv, O.M.; Gurianov, Y.; Serkiz, R.Y.; Klepach, H.M.; Gonchar, M.V.; Nisnevitch, M. "Green" Prussian Blue Analogues as Peroxidase Mimetics for Amperometric Sensing and Biosensing. *Biosensors* **2021**, *11*, 193. [CrossRef] [PubMed]
40. Ishizaki, M.; Ohshida, E.; Tanno, H.; Kawamoto, T.; Tanaka, H.; Hara, K.; Kominami, H.; Kurihara, M. H_2O_2-sensing abilities of mixed-metal (Fe-Ni) Prussian blue analogs in a wide pH range. *Inorg. Chim. Acta* **2020**, *502*, 119314. [CrossRef]
41. Uematsu, K.; Ueno, T.; Katano, H. Effect of Poly-l-lysine on a Glucose Sensor Based on Glucose Oxidase and Ferricyanide Ion. *Anal. Sci.* **2018**, *34*, 947–951. [CrossRef]
42. Garjonyte, R.; Malinauskas, A. Operational stability of amperometric hydrogen peroxide sensors, based on ferrous and copper hexacyanoferrates. *Sens. Actuators B Chem.* **1999**, *56*, 93–97. [CrossRef]
43. Karyakin, A.A. Advances of Prussian blue and its analogues in (bio)sensors. *Curr. Opin. Electrochem.* **2017**, *5*, 92–98. [CrossRef]
44. Komkova, M.A.; Zarochintsev, A.A.; Karyakina, E.E.; Karyakin, A.A. Electrochemical and sensing properties of Prussian Blue based nanozymes "artificial peroxidase". *J. Electroanal. Chem.* **2020**, *872*, 114048. [CrossRef]
45. Schrattenecker, J.D.; Heer, R.; Melnik, E.; Maier, T.; Fafilek, G.; Hainberger, R. Hexaammineruthenium(II)/(III) as alternative redox-probe to Hexacyanoferrat(II)/(III) for stable impedimetric biosensing with gold electrodes. *Biosens. Bioelectron.* **2019**, *127*, 25–30. [CrossRef] [PubMed]
46. Sharma, D.; Lim, Y.; Lee, Y.; Shin, H. Glucose sensor based on redox-cycling between selectively modified and unmodified combs of carbon interdigitated array nanoelectrodes. *Anal. Chim. Acta* **2015**, *889*, 194–202. [CrossRef]

47. Nakabayashi, Y.; Omayu, A.; Morii, S.; Yagi, S. Evaluation of osmium(II) complexes as mediators accessible for biosensors. *Sens. Actuators B Chem.* **2000**, *66*, 128–130. [CrossRef]
48. Zakeeruddin, S.M.; Fraser, D.M.; Nazeeruddin, M.K.; Grätzel, M. Towards mediator design: Characterization of tris-(4,4′-substituted-2,2′-bipyridine) complexes of iron(II), ruthenium(II) and osmium(II) as mediators for glucose oxidase of Aspergillus niger and other redox proteins. *J. Electroanal. Chem.* **1992**, *337*, 253–283. [CrossRef]
49. Salinas, E.; Torriero, A.A.J.; Battaglini, F.; Sanz, M.I.; Olsina, R.; Raba, J. Continuous-flow/stopped-flow system for enzyme immunoassay using a rotating bioreactor: Determination of Chagas disease. *Biosens. Bioelectron.* **2005**, *21*, 313–321. [CrossRef]
50. Calhoun, M.C.; Stachurski, C.D.; Winn, S.L.; Gizzie, E.A.; Daniel, A.W.; Schley, N.D.; Cliffel, D.E. Trace Oxygen Affects Osmium Redox Polymer Synthesis for Wired Enzymatic Biosensors. *J. Electrochem. Soc.* **2022**, *169*, 016506. [CrossRef]
51. Torriero, A.A.J. Comments and Protocols for the Construction and Calibration of Ag/AgCl Reference Electrodes. *Int. J. Biochem. Physiol.* **2023**, *8*, 000219. [CrossRef]
52. Meites, L. Handbook of analytical chemistry. *Soil Sci.* **1963**, *96*, 358. [CrossRef]
53. Ohara, T.J.; Rajagopalan, R.; Heller, A. Glucose electrodes based on cross-linked $[Os(bpy)_2Cl]^{+/2+}$ complexed poly(1-vinylimidazole) films. *Anal. Chem.* **1993**, *65*, 3512–3517. [CrossRef] [PubMed]
54. Bennett, R.; Leech, D. Improved operational stability of mediated glucose enzyme electrodes for operation in human physiological solutions. *Bioelectrochemistry* **2020**, *133*, 107460. [CrossRef]
55. Lielpetere, A.; Jayakumar, K.; Leech, D.; Schuhmann, W. Cross-linkable polymer-based multi-layers for protecting electrochemical glucose biosensors against uric acid, ascorbic acid, and biofouling interferences. *ACS Sens.* **2023**, *8*, 1756–1765. [CrossRef] [PubMed]
56. Navarro-Nateras, L.; Diaz-Gonzalez, J.; Aguas-Chantes, D.; Coria-Oriundo, L.L.; Battaglini, F.; Ventura-Gallegos, J.L.; Zentella-Dehesa, A.; Oza, G.; Arriaga, L.G.; Casanova-Moreno, J.R. Development of a Redox-Polymer-Based Electrochemical Glucose Biosensor Suitable for Integration in Microfluidic 3D Cell Culture Systems. *Biosensors* **2023**, *13*, 582. [CrossRef]
57. Danilowicz, C.; Cortón, E.; Battaglini, F. Osmium complexes bearing functional groups: Building blocks for integrated chemical systems. *J. Electroanal. Chem.* **1998**, *445*, 89–94. [CrossRef]
58. Jayakumar, K.; Bennett, R.; Leech, D. Electrochemical glucose biosensor based on an osmium redox polymer and glucose oxidase grafted to carbon nanotubes: A design-of-experiments optimisation of current density and stability. *Electrochim. Acta* **2021**, *371*, 137845. [CrossRef]
59. Conghaile, P.O.; Kamireddy, S.; MacAodha, D.; Kavanagh, P.; Leech, D. Mediated glucose enzyme electrodes by cross-linking films of osmium redox complexes and glucose oxidase on electrodes. *Anal. Bioanal. Chem.* **2013**, *405*, 3807–3812. [CrossRef]
60. Schuvailo, O.N.; Dzyadevych, S.V.; El'skaya, A.V.; Gautier-Sauvigné, S.; Csöregi, E.; Cespuglio, R.; Soldatkin, A.P. Carbon fibre-based microbiosensors for in vivo measurements of acetylcholine and choline. *Biosens. Bioelectron.* **2005**, *21*, 87–94. [CrossRef]
61. Kirthiga, M.; Rajendran, L.; Fernandez, C. Theoretical treatment of diffusion and kinetics of osmium redox polymer mediated glucose oxidase enzyme electrodes: Analytical expression of current density for varying potential. *Electrochim. Acta* **2017**, *230*, 89–97. [CrossRef]
62. Alpeeva, I.S.; Soukharev, V.S.; Alexandrova, L.; Shilova, N.V.; Bovin, N.V.; Csöregi, E.; Ryabov, A.D.; Sakharov, I.Y. Cyclometalated ruthenium(II) complexes as efficient redox mediators in peroxidase catalysis. *J. Biol. Inorg. Chem.* **2003**, *8*, 683–688. [CrossRef]
63. Rivera, N.; Colón, Y.; Guadalupe, A.R. Ruthenium complexes as redox mediators for malate and lactate dehydrogenases. *Bioelectrochem. Bioenerg.* **1994**, *34*, 169–175. [CrossRef]
64. Deng, H.; Teo, A.K.L.; Gao, Z. An interference-free glucose biosensor based on a novel low potential redox polymer mediator. *Sens. Actuators B Chem.* **2014**, *191*, 522–528. [CrossRef]
65. Yamamoto, K.; Zeng, H.; Shen, Y.; Ahmed, M.M.; Kato, T. Evaluation of an amperometric glucose biosensor based on a ruthenium complex mediator of low redox potential. *Talanta* **2005**, *66*, 1175–1180. [CrossRef] [PubMed]
66. Park, S.-B.; Jeon, W.-Y.; Choi, Y.-B. Electrochemical Glucose Sensing by Using Glucose Dehydrogenase Enzyme and the Synthesized Poly-ruthenium Mediator. *Polymer* **2023**, *47*, 171–180. [CrossRef]
67. Costa-Rama, E.; Fernández Abedul, M.T. Chapter 3—Electrochemical behavior of the redox probe hexaammineruthenium(III) ($[Ru(NH_3)_6]^{3+}$) using voltammetric techniques. In *Laboratory Methods in Dynamic Electroanalysis*; Fernandez Abedul, M.T., Ed.; Elsevier: Amsterdam, The Netherlands, 2020; pp. 25–33.
68. Han, Y.D.; Jang, Y.H.; Yoon, H.C. Cascadic Multienzyme Reaction-Based Electrochemical Biosensors. In *Biosensors Based on Aptamers and Enzymes*; Gu, M.B., Kim, H.-S., Eds.; Springer: Berlin/Heidelberg, Germany, 2014; pp. 221–251.
69. Raymundo-Pereira, P.; Mascarenhas, A.; Teixeira, M. Evaluation of the Oxo-bridged Dinuclear Ruthenium Ammine Complex as Redox Mediator in an Electrochemical Biosensor. *Electroanalysis* **2015**, *28*, 562–569. [CrossRef]
70. Hromadová, M.; Fawcett, W.R. Studies of double-layer effects at single-crystal gold electrodes. 1. The reduction kinetics of hexaamminecobalt (III) ion in aqueous solutions. *J. Phys. Chem. A* **2000**, *104*, 4356–4363. [CrossRef]
71. Martín-Yerga, D.; Costa Rama, E.; Costa Garcia, A. Electrochemical study and determination of electroactive species with screen-printed electrodes. *J. Chem. Educ.* **2016**, *93*, 1270–1276. [CrossRef]

72. Vijaikanth, V.; Li, G.; Swaddle, T.W. Kinetics of reduction of aqueous hexaammineruthenium (III) Ion at Pt and Au microelectrodes: Electrolyte, temperature, and pressure effects. *Inorg. Chem.* **2013**, *52*, 2757–2768. [CrossRef]
73. Gajdosova, V.P.; Lorencova, L.; Kasak, P.; Jerigova, M.; Velic, D.; Orovcik, L.; Barath, M.; Farkas, P.; Tkac, J. Redox features of hexaammineruthenium(III) on MXene modified interface: Three options for affinity biosensing. *Anal. Chim. Acta* **2022**, *1227*, 340310. [CrossRef] [PubMed]
74. Quan, C.; Zhang, Y.; Liu, Y.; Wen, L.; Yang, H.; Huang, X.; Yang, M.; Xu, B. Electrochemical Glucose Sensor Based on Dual Redox Mediators. *Biosensors* **2025**, *15*, 9. [CrossRef]
75. Ayankojo, A.G.; Reut, J.; Boroznjak, R.; Syritski, V. Ruthenium oxide electrode integrated with molecularly imprinted polymer for direct electrochemical sensing of a neurotrophic factor protein. *Sens. Actuators B Chem.* **2025**, *429*, 137301. [CrossRef]
76. Schachinger, F.; Ma, S.; Ludwig, R. Redox potential of FAD-dependent glucose dehydrogenase. *Electrochem. Commun.* **2023**, *146*, 107405. [CrossRef]
77. Mashazi, P.N.; Ozoemena, K.I.; Nyokong, T. Tetracarboxylic acid cobalt phthalocyanine SAM on gold: Potential applications as amperometric sensor for H_2O_2 and fabrication of glucose biosensor. *Electrochim. Acta* **2006**, *52*, 177–186. [CrossRef]
78. Ozoemena, K.I. Anodic oxidation and amperometric sensing of hydrazine at a glassy carbon electrode modified with cobalt(II) phthalocyanine–cobalt(II) tetraphenylporphyrin (CoPc-$(CoTPP)_4$) supramolecular complex. *Sensors* **2006**, *6*, 874–891. [CrossRef]
79. Ozoemena, K.I.; Zhao, Z.; Nyokong, T. Immobilized cobalt(II) phthalocyanine–cobalt(II) porphyrin pentamer at a glassy carbon electrode: Applications to efficient amperometric sensing of hydrogen peroxide in neutral and basic media. *Electrochem. Commun.* **2005**, *7*, 679–684. [CrossRef]
80. Rahim, A.; Santos, L.S.S.; Barros, S.B.A.; Kubota, L.T.; Gushikem, Y. Dissolved O_2 sensor based on cobalt(II) phthalocyanine immobilized in situ on electrically conducting carbon ceramic mesoporous SiO_2/C material. *Sens. Actuators B Chem.* **2013**, *177*, 231–238. [CrossRef]
81. Yuan, B.; Sun, P.; Fernandez, C.; Wang, H.; Guan, P.; Xu, H.; Niu, Y. Molecular fluorinated cobalt phthalocyanine immobilized on ordered mesoporous carbon as an electrochemical sensing platform for sensitive detection of hydrogen peroxide and hydrazine in alkaline medium. *J. Electroanal. Chem.* **2022**, *906*, 116019. [CrossRef]
82. Hsu, C.-Y.; Sato, T.; Moriyama, S.; Higuchi, M. A Co(II)-based metallo-supramolecular polymer as a novel enzyme immobilization matrix for electrochemical glucose biosensing. *Eur. Polym. J.* **2016**, *83*, 499–506. [CrossRef]
83. Shu, J.; Qiu, Z.; Wei, Q.; Zhuang, J.; Tang, D. Cobalt-Porphyrin-Platinum-Functionalized Reduced Graphene Oxide Hybrid Nanostructures: A Novel Peroxidase Mimetic System for Improved Electrochemical Immunoassay. *Sci. Rep.* **2015**, *5*, 15113. [CrossRef] [PubMed]
84. Sánchez-Calvo, A.; Costa-García, A.; Blanco-López, M.C. Paper-based electrodes modified with cobalt phthalocyanine colloid for the determination of hydrogen peroxide and glucose. *Analyst* **2020**, *145*, 2716–2724. [CrossRef]
85. Prabhu, C.K.; Naveen, K.; Aralekallu, S. Shivalingayya and LK Sannegowda. *RSC Sustain.* **2023**, *1*, 128–138. [CrossRef]
86. Yaqub, A.; Gilani, S.R.; Bilal, S.; Hayat, A.; Asif, A.; Siddique, S.A. Efficient preparation of a nonenzymatic nanoassembly based on cobalt-substituted polyoxometalate and polyethylene imine-capped silver nanoparticles for the electrochemical sensing of carbofuran. *ACS Omega* **2022**, *7*, 149–159. [CrossRef] [PubMed]
87. Zhang, X.; Wang, S.; Shen, Q. The electrochemical behavior of p-aminophenol at a ω-mercaptopropionic acid self-assembled gold electrode. *Microchim. Acta* **2005**, *149*, 37–42. [CrossRef]
88. Katz, E.; Shipway, A.N.; Willner, I. Bioelectrochemistry. In *Encyclopedia of Electrochemistry, Volume 9: Bioelectrochemistry*; Bard, A.J., Stratmann, M., Steckhan, E., Eds.; Wiley-VCH: Weinheim, Germany, 2002; Volume 9, pp. 559–626.
89. Laviron, E.; Roullier, L. Electrochemical reactions with protonations at equilibrium: Part IX. Comparison between the surface and heterogeneous electrochemical rate constants in the system phenazine/dihydrophenazine. *J. Electroanal. Chem. Interfacial Electrochem.* **1983**, *157*, 7–18. [CrossRef]
90. Savéant, J.-M. Molecular catalysis of electrochemical reactions. *Mechanistic aspects. Chem. Rev.* **2008**, *108*, 2348–2378. [CrossRef]
91. Papadakis, R. Mono- and Di-Quaternized 4,4′-Bipyridine Derivatives as Key Building Blocks for Medium- and Environment-Responsive Compounds and Materials. *Molecules* **2020**, *25*, 1. [CrossRef]
92. Bockris, J.O.M.; Reddy, A.K.; Gamboa-Aldeco, M. *Modern Electrochemistry 2A: Fundamentals of Electrodics*; Springer: Berlin/Heidelberg, Germany, 2000.
93. Cook, S.K.; Horrocks, B.R. Heterogeneous electron-transfer rates for the reduction of viologen derivatives at platinum and bismuth electrodes in acetonitrile. *ChemElectroChem* **2017**, *4*, 320–331. [CrossRef]
94. Vaid, T.P.; Sanford, M.S. An organic super-electron-donor as a high energy density negative electrolyte for nonaqueous flow batteries. *Chem. Commun.* **2019**, *55*, 11037–11040. [CrossRef] [PubMed]
95. Burešová, Z.; Klikar, M.; Mazúr, P.; Mikešová, M.; Kvíčala, J.; Bystron, T.; Bureš, F. Redox Property Tuning in Bipyridinium Salts. *Front. Chem.* **2021**, *8*, 2020. [CrossRef] [PubMed]
96. Naz, L.; Mohammad, M. Kinetics of Dimerization of the Reduced Products of Methyl Viologen Dication. *J. Chem. Soc. Pak.* **2017**, *39*, 4.

97. Shah, K.W.; Wang, S.-X.; Soo, D.X.Y.; Xu, J. Viologen-based electrochromic materials: From small molecules, polymers and composites to their applications. *Polymers* **2019**, *11*, 1839. [CrossRef]
98. Jarošová, R.; De Sousa Bezerra, P.M.; Munson, C.; Swain, G.M. Assessment of heterogeneous electron-transfer rate constants for soluble redox analytes at tetrahedral amorphous carbon, boron-doped diamond, and glassy carbon electrodes. *Phys. Status Solidi A* **2016**, *213*, 2087–2098. [CrossRef]
99. Randviir, E.P. A cross examination of electron transfer rate constants for carbon screen-printed electrodes using Electrochemical Impedance Spectroscopy and cyclic voltammetry. *Electrochim. Acta* **2018**, *286*, 179–186. [CrossRef]
100. Chen, L.; Lin, C.; Compton, R.G. Single entity electrocatalysis: Oxygen reduction mediated via methyl viologen doped Nafion nanoparticles. *Phys. Chem. Chem. Phys.* **2018**, *20*, 15795–15806. [CrossRef] [PubMed]
101. Easley, A.D.; Li, C.-H.; Li, S.-G.; Nguyen, T.P.; Mick Kuo, K.-H.; Wooley, K.L.; Tabor, D.P.; Lutkenhaus, J.L. Electron transport kinetics for viologen-containing polypeptides with varying side group linker spacing. *J. Mater. Chem. A* **2024**, *12*, 31871–31882. [CrossRef]
102. Oughli, A.A.; Vélez, M.; Birrell, J.A.; Schuhmann, W.; Lubitz, W.; Plumeré, N.; Rüdiger, O. Viologen-modified electrodes for protection of hydrogenases from high potential inactivation while performing H_2 oxidation at low overpotential. *Dalton Trans.* **2018**, *47*, 10685–10691. [CrossRef]
103. Song, J.; Hong, Z.; Koh, A.; Shin, W. Covalent Immobilization of Diaphorase in Viologen Polymer Network for Highly Sensitive Detection of NAD^+ and NADH. *J. Electrochem. Sci. Technol.* **2014**, *5*, 19–22. [CrossRef]
104. Mruthunjaya, A.K.V.; Torriero, A.A.J. Mechanistic Aspects of the Electrochemical Oxidation of Aliphatic Amines and Aniline Derivatives. *Molecules* **2023**, *28*, 471. [CrossRef]
105. Chandra, S.; Lielpetere, A.; Schuhmann, W. Designing a high-potential metal-free viologen-based redox polymer for effective wiring of FAD-dependent glucose dehydrogenase. *Sens. Actuators B Chem.* **2023**, *397*, 134660. [CrossRef]
106. Koomson, D.A.; Nicholson, J.H.; Brogan, A.P.S.; Aldous, L. Re-assessing viologens for modern bio-electrocatalysis. *Chem. Sci.* **2024**, *15*, 9325–9332. [CrossRef] [PubMed]
107. Ghica, M.E.; Brett, C.M.A. A glucose biosensor using methyl viologen redox mediator on carbon film electrodes. *Anal. Chim. Acta* **2005**, *532*, 145–151. [CrossRef]
108. Raymo, F.M.; Alvarado, R.J.; Pacsial, E.J. Electroactive films incorporating 4,4′-Bipyridinium building blocks. *J. Supramol. Chem.* **2002**, *2*, 63–77. [CrossRef]
109. Furota, S.; Kaneko, M.; Tsujimura, S.; Takeshita, D.; Nakamichi, Y.; Igarashi, K.; Nobu, M.K.; Yoshikawa, M.; Asahina, K.; Fukaya, C.; et al. Bidirectional electro-enzymatic reaction of coenzyme F420 using benzyl viologen and F420-dependent sulfite reductase. *Bioelectrochemistry* **2025**, *164*, 108922. [CrossRef] [PubMed]
110. Bus, J.S.; Gibson, J.E. Paraquat: Model for oxidant-initiated toxicity. *Environ. Health Perspect.* **1984**, *55*, 37–46. [CrossRef] [PubMed]
111. Huang, B.; Gao, S.; Xu, Z.; He, H.; Pan, X. The Functional Mechanisms and Application of Electron Shuttles in Extracellular Electron Transfer. *Curr. Microbiol.* **2018**, *75*, 99–106. [CrossRef]
112. Rhodes, Z.; Simoska, O.; Dantanarayana, A.; Stevenson, K.J.; Minteer, S.D. Using structure-function relationships to understand the mechanism of phenazine-mediated extracellular electron transfer in *Escherichia coli*. *iScience* **2021**, *24*, 103033. [CrossRef] [PubMed]
113. Fitriana, M.; Hiraka, K.; Ikebukuro, K.; Sode, K.; Tsugawa, W. A Thiol-reactive Phenazine Ethosulfate: A Novel Redox Mediator for Quasi-direct Electron-transfer-type Sensors. *Sens. Mater.* **2022**, *34*, 2105–2124. [CrossRef]
114. Ricci, F.; Amine, A.; Moscone, D.; Palleschi, G. A probe for NADH and H_2O_2 amperometric detection at low applied potential for oxidase and dehydrogenase based biosensor applications. *Biosens. Bioelectron.* **2007**, *22*, 854–862. [CrossRef]
115. Hatada, M.; Loew, N.; Inose-Takahashi, Y.; Okuda-Shimazaki, J.; Tsugawa, W.; Mulchandani, A.; Sode, K. Development of a glucose sensor employing quick and easy modification method with mediator for altering electron acceptor preference. *Bioelectrochemistry* **2018**, *121*, 185–190. [CrossRef] [PubMed]
116. Yabuki, S.; Fumio, M.; Asai, M. Preparation and characterization of an electroconductive membrane containing glutamate dehydrogenase, NADP, and mediator. *Biosens. Bioelectron.* **1991**, *6*, 311–315. [CrossRef]
117. Bartlett, P.N.; Birkin, P.R.; Palmisano, F.; De Benedetto, G. A study on the direct electrochemical communication between horseradish peroxidase and a poly(aniline) modified electrode. *J. Chem. Soc. Faraday Trans.* **1996**, *92*, 3123–3130. [CrossRef]
118. Barsan, M.M.; Ghica, M.E.; Brett, C.M.A. Electrochemical sensors and biosensors based on redox polymer/carbon nanotube modified electrodes: A review. *Anal. Chim. Acta* **2015**, *881*, 1–23. [CrossRef]
119. Gannett, C.N.; Peterson, B.M.; Shen, L.; Seok, J.; Fors, B.P.; Abruña, H.D. Cross-linking Effects on Performance Metrics of Phenazine-Based Polymer Cathodes. *ChemSusChem* **2020**, *13*, 2428–2435. [CrossRef]
120. Sanderson, D.G.; Gross, E.L.; Seibert, M. A photosynthetic photoelectrochemical cell using phenazine methosulfate and phenazine ethosulfate as electron acceptors. *Appl. Biochem. Biotechnol.* **1987**, *14*, 1–20. [CrossRef]
121. Crooks, R.M.; Bard, A.J. Electrochemistry in near-critical and supercritical fluids: Part VI. The electrochemistry of ferrocene and phenazine in acetonitrile between 25 and 300 °C. *J. Electroanal. Chem. Interfacial Electrochem.* **1988**, *243*, 117–131. [CrossRef]

122. Vicente, F.; Roig, A.; Garcia-Jarefio, J.J.; Trijueque, J.; Navarro-Laboulais, J.; Scholl, H. Electrode Processes of Neutral Red on Glassy Carbon and Indium Tin Oxide (ITO) Electrodes in Aqueous Buffered Solutions. *Port. Electrochim. Acta* **1995**, *13*, 137–152.
123. Halaka, F.G.; Babcock, G.T.; Dye, J.L. Properties of 5-methylphenazinium methyl sulfate. Reaction of the oxidized form with NADH and of the reduced form with oxygen. *J. Biol. Chem.* **1982**, *257*, 1458–1461. [CrossRef]
124. Hisada, R.; Yagi, T. 1-Methoxy-5-Methylphenazinium Methyl Sulfate: A Photochemically Stable Electron Mediator between NADH and Various Electron Acceptors1. *J. Biochem.* **1977**, *82*, 1469–1473. [CrossRef]
125. Jahn, B.; Jonasson, N.S.W.; Hu, H.; Singer, H.; Pol, A.; Good, N.M.; den Camp, H.J.M.O.; Martinez-Gomez, N.C.; Daumann, L.J. Understanding the chemistry of the artificial electron acceptors PES, PMS, DCPIP and Wurster's Blue in methanol dehydrogenase assays. *J. Biol. Inorg. Chem.* **2020**, *25*, 199–212. [CrossRef] [PubMed]
126. Kalimuthu, P.; Leimkühler, S.; Bernhardt, P.V. Catalytic electrochemistry of xanthine dehydrogenase. *J. Phys. Chem. B* **2012**, *116*, 11600–11607. [CrossRef] [PubMed]
127. Nagata, M.; Lee, J.; Henley, S.; Ikebukuro, K.; Sode, K. An Amine-Reactive Phenazine Ethosulfate (arPES)—A Novel Redox Probe for Electrochemical Aptamer-Based Sensor. *Sensors* **2022**, *22*, 1760. [CrossRef]
128. Li, S.; De Groote Tavares, C.; Tolar, J.G.; Ajo-Franklin, C.M. Selective bioelectronic sensing of pharmacologically relevant quinones using extracellular electron transfer in Lactiplantibacillus plantarum. *Biosens. Bioelectron.* **2024**, *243*, 115762. [CrossRef]
129. Longatte, G.; Buriez, O.; Labbé, E.; Guille-Collignon, M.; Lemaître, F. Electrochemical Behavior of Quinones Classically Used for Bioenergetical Applications: Considerations and Insights about the Anodic Side. *ChemElectroChem* **2024**, *11*, e202300542. [CrossRef]
130. Xu, N.; Wang, T.-L.; Li, W.-J.; Wang, Y.; Chen, J.-J.; Liu, J. Tuning Redox Potential of Anthraquinone-2-Sulfonate (AQS) by Chemical Modification to Facilitate Electron Transfer from Electrodes in Shewanella Oneidensis. *Front. Bioeng. Biotechnol.* **2021**, *9*, 2021. [CrossRef] [PubMed]
131. Ruiz-Diaz, J.J.J.; Torriero, A.A.J.; Salinas, E.; Marchevsky, E.J.; Sanz, M.I.; Raba, J. Enzymatic rotating biosensor for cysteine and glutathione determination in a FIA system. *Talanta* **2006**, *68*, 1343–1352. [CrossRef]
132. Torriero, A.A.J.; Salinas, E.; Marchevsky, E.J.; Raba, J.; Silber, J.J. Penicillamine determination using a tyrosinase micro-rotating biosensor. *Anal. Chim. Acta* **2006**, *580*, 136–142. [CrossRef]
133. Torriero, A.A.J.; Salinas, E.; Raba, J.; Silber, J.J. Sensitive determination of ciprofloxacin and norfloxacin in biological fluids using an enzymatic rotating biosensor. *Biosens. Bioelectron.* **2006**, *22*, 109–115. [CrossRef]
134. Torriero, A.A.J. Electrochemical oxidation of catechol in the presence of methimazole: Application of square-wave voltammetric detection of methimazole to pharmaceutical formulations. *Med. Anal. Chem. Int. J.* **2019**, *3*, 000139. [CrossRef]
135. Guin, P.; Das, S.; Mandal, P. Electrochemical Reduction of Quinones in Different Media: A Review. *SAGE-Hindawi Access Res. Int. J. Electrochem.* **2011**, *22*, 816202. [CrossRef]
136. Deakin, M.R.; Wightman, R.M. The kinetics of some substituted catechol/o-quinone couples at a carbon paste electrode. *J. Electroanal. Chem. Interfacial Electrochem.* **1986**, *206*, 167–177. [CrossRef]
137. DuVall, S.H.; McCreery, R.L. Control of catechol and hydroquinone electron-transfer kinetics on native and modified glassy carbon electrodes. *Anal. Chem.* **1999**, *71*, 4594–4602. [CrossRef]
138. Kim, R.S.; Chung, T.D. The Electrochemical Reaction Mechanism and Applications of Quinones. *Bull. Korean Chem. Soc.* **2014**, *35*, 3143–3155. [CrossRef]
139. Tessensohn, M.E.; Hirao, H.; Webster, R.D. Electrochemical properties of phenols and quinones in organic solvents are strongly influenced by hydrogen-bonding with water. *J. Phys. Chem. C* **2013**, *117*, 1081–1090. [CrossRef]
140. Silva, P.S.D.; Gasparini, B.C.; Magosso, H.A.; Spinelli, A. Electrochemical behavior of hydroquinone and catechol at a silsesquioxane-modified carbon paste electrode. *J. Braz. Chem. Soc.* **2013**, *24*, 695–699. [CrossRef]
141. Halpin, G.; Herdman, K.; Dempsey, E. Electrochemical investigations into enzymatic polymerisation of 1,10-phenanthroline-5,6-dione as a redox mediator for lactate sensing. *Sens. Actuators Rep.* **2021**, *3*, 100032. [CrossRef]
142. Kausaite-Minkstimiene, A.; Simanaityte, R.; Ramanaviciene, A.; Glumbokaite, L.; Ramanavicius, A. Reagent-less amperometric glucose biosensor based on a graphite rod electrode layer-by-layer modified with 1,10-phenanthroline-5,6-dione and glucose oxidase. *Talanta* **2017**, *171*, 204–212. [CrossRef]
143. Zor, E.; Oztekin, Y.; Mikoliunaite, L.; Voronovic, J.; Ramanaviciene, A.; Anusevicius, Z.; Bingol, H.; Ramanavicius, A. 1,10-Phenanthroline-5,6-dione and 9,10-phenanthrenequinone as redox mediators for amperometric glucose biosensors. *J. Solid State Electrochem.* **2014**, *18*, 1529–1536. [CrossRef]
144. Genys, P.; Aksun, E.; Tereshchenko, A.; Valiūnienė, A.; Ramanaviciene, A.; Ramanavicius, A. Electrochemical Deposition and Investigation of Poly-9,10-Phenanthrenequinone Layer. *Nanomaterials* **2019**, *9*, 702. [CrossRef]
145. German, N.; Popov, A.; Ramanaviciene, A. The Development and Evaluation of Reagentless Glucose Biosensors Using Dendritic Gold Nanostructures as a Promising Sensing Platform. *Biosensors* **2023**, *13*, 727. [CrossRef]
146. Bolton, J.L.; Trush, M.A.; Penning, T.M.; Dryhurst, G.; Monks, T.J. Role of quinones in toxicology. *Chem. Res. Toxicol.* **2000**, *13*, 135–160. [CrossRef] [PubMed]

147. Cohen, R.; Cohen, Y.; Mukha, D.; Yehezkeli, O. Oxygen insensitive amperometric glucose biosensor based on FAD dependent glucose dehydrogenase co-entrapped with DCPIP or DCNQ in a polydopamine layer. *Electrochim. Acta* **2021**, *367*, 137477. [CrossRef]
148. Marchesiello, M.; Geniés, E.M. Glucose sensor: Polypyrrole-glucose oxidase elecrtode in the presence of p-benzoquinone. *Electrochim. Acta* **1992**, *37*, 1987–1992. [CrossRef]
149. El Atrash, S.S.; O'Neill, R.D. Characterisation in vitro of a naphthoquinone-mediated glucose oxidase-modified carbon paste electrode designed for neurochemical analysis in vivo. *Electrochim. Acta* **1995**, *40*, 2791–2797. [CrossRef]
150. Tang, H.T.; Lunte, C.E.; Halsall, H.B.; Heineman, W.R. p-aminophenyl phosphate: An improved substrate for electrochemical enzyme immnoassay. *Anal. Chim. Acta* **1988**, *214*, 187–195. [CrossRef]
151. Beiginejad, H.; Nematollahi, D.; Varmaghani, F. Electrochemical oxidation of some aminophenols in various pHs. *J. Electrochem. Soc.* **2013**, *160*, H41. [CrossRef]
152. Salavagione, H.J.; Arias, J.; Garcés, P.; Morallón, E.; Barbero, C.; Vázquez, J.L. Spectroelectrochemical study of the oxidation of aminophenols on platinum electrode in acid medium. *J. Electroanal. Chem.* **2004**, *565*, 375–383. [CrossRef]
153. Jackowska, K.; Bukowska, J.; Kudelski, A. Electro-oxidation of o-aminophenol studied by cyclic voltammetry and surface enhanced Raman scattering (SERS). *J. Electroanal. Chem.* **1993**, *350*, 177–187. [CrossRef]
154. Zhang, S.; Jiao, K.; Chen, H.; Wang, M. Detection of ferritin in human serum with a MAP–H_2O_2–HRP voltammetric enzyme-linked immunoassay system. *Talanta* **1999**, *50*, 95–101. [CrossRef]
155. Kava, A.A.; Henry, C.S. Exploring carbon particle type and plasma treatment to improve electrochemical properties of stencil-printed carbon electrodes. *Talanta* **2021**, *221*, 121553. [CrossRef]
156. Zhang, J.; Yao, S.; Nie, L.; Wei, W. Evaluation of the kinetic parameters of first-order reactions following charge transfer by applying a long-path-length spectroelectrochemical technique. *Anal. Sci.* **2000**, *16*, 87–91. [CrossRef]
157. Puiu, M.; Răducan, A.; Babaligea, I.; Oancea, D. Oxidase–peroxidase reaction: Kinetics of peroxidase-catalysed oxidation of 2-aminophenol. *Bioprocess Biosyst. Eng.* **2008**, *31*, 579–586. [CrossRef]
158. Sayyah, S.M.; El-Rabiey, M.M.; El-Rehim, S.S.A.; Azooz, R.E. Electropolymerization kinetics of o-aminophenol and characterization of the obtained polymer films. *J. Appl. Polym. Sci.* **2006**, *99*, 3093–3109. [CrossRef]
159. Tucceri, R.; Arnal, P.M.; Scian, A.N. Spectroscopic Characterization of Poly(ortho-Aminophenol) Film Electrodes: A Review Article. *J. Spectrosc.* **2013**, *2013*, 951604. [CrossRef]
160. Das, J.; Jo, K.; Lee, J.W.; Yang, H. Electrochemical Immunosensor Using p-Aminophenol Redox Cycling by Hydrazine Combined with a Low Background Current. *Anal. Chem.* **2007**, *79*, 2790–2796. [CrossRef] [PubMed]
161. Mruthunjaya, A.K.V.; Chatelier, R.C.; Torriero, A.A.J. Electrochemical Disposable Biosensor to Monitor Dabigatran in Point-of-Care Anticoagulation Therapy. *Molecules* **2023**, *28*, 4953. [CrossRef]
162. Mruthunjaya, A.K.V.; Chatelier, R.C.; Torriero, A.A.J. Calibration-free electrochemical sensor to monitor factor-Xa inhibitors at the point-of-care anticoagulation therapy. *Talanta* **2024**, *270*, 125593. [CrossRef]
163. Mruthunjaya, A.K.V.; Hodges, A.M.; Chatelier, R.C.; Torriero, A.A.J. Calibration-Free Disposable Electrochemical Sensor with Co-Facing Electrodes: Theory and Characterisation with Fixed and Changing Mediator Concentration. *Electrochim. Acta* **2023**, *460*, 142596. [CrossRef]
164. Miland, E.; Miranda Ordieres, A.J.; Tuñón Blanco, P.; Smyth, M.R.; Fágáin, C.Ó. Poly(o-aminophenol)-modified bienzyme carbon paste electrode for the detection of uric acid. *Talanta* **1996**, *43*, 785–796. [CrossRef]
165. Pariente, F.; Hernández, L.; Abruña, H.D.; Lorenzo, E. Alkaline phosphatase-modified carbon fibre disc microelectrode for the determination of 4-aminophenyl phosphate. *Anal. Chim. Acta* **1993**, *273*, 187–193. [CrossRef]
166. Pan, D.; Chen, J.; Nie, L.; Tao, W.; Yao, S. Amperometric glucose biosensor based on immobilization of glucose oxidase in electropolymerized o-aminophenol film at Prussian blue-modified platinum electrode. *Electrochim. Acta* **2004**, *49*, 795–801. [CrossRef]
167. Tian, F.; Greplová, M.; Frébort, I.; Dale, N.; Napier, R. A Highly Selective Biosensor with Nanomolar Sensitivity Based on Cytokinin Dehydrogenase. *PLoS ONE* **2014**, *9*, e90877. [CrossRef]
168. Josephy, P.D.; Eling, T.E.; Mason, R.P. Oxidation of p-aminophenol catalyzed by horseradish peroxidase and prostaglandin synthase. *Mol. Pharmacol.* **1983**, *23*, 461–466. [CrossRef]
169. Sanghavi, B.J.; Wolfbeis, O.S.; Hirsch, T.; Swami, N.S. Nanomaterial-based electrochemical sensing of neurological drugs and neurotransmitters. *Microchim. Acta* **2015**, *182*, 1–41. [CrossRef] [PubMed]
170. Kulys, J.; Hansen, H.E.; Buch-Rasmussen, T.; Wang, J.; Ozsoz, M. Glucose biosensor based on the incorporation of Meldola Blue. *Anal. Chim. Acta* **1994**, *288*, 193–196. [CrossRef]
171. Hammerich, O.; Speiser, B. *Organic Electrochemistry*; CRC Press: Boca Raton, FL, USA, 2016.
172. Çakir, S.; Arslan, E.Y. Voltammetry of resazurin at a mercury electrode. *Chem. Pap.* **2010**, *64*, 386–394. [CrossRef]
173. Khazalpour, S.; Nematollahi, D. Electrochemical study of Alamar Blue (resazurin) in aqueous solutions and room-temperature ionic liquid 1-butyl-3-methylimidazolium tetrafluoroborate at a glassy carbon electrode. *RSC Adv.* **2014**, *4*, 8431–8438. [CrossRef]

174. Ni, F.; Feng, H.; Gorton, L.; Cotton, T.M. Electrochemical and SERS studies of chemically modified electrodes: Nile Blue A, a mediator for NADH oxidation. *Langmuir* **1990**, *6*, 66–73. [CrossRef]
175. Papeschi, G.; Costa, M.; Bordi, S. Electrochemical behavior of methylene blue and its leucoform at the mercury electrode. *J. Electrochem. Soc.* **1981**, *128*, 1518. [CrossRef]
176. Svitková, V.; Vyskočil, V. Electrochemical behavior of methylene blue at bare and DNA-modified silver solid amalgam electrodes. *J. Solid State Electrochem.* **2022**, *26*, 2491–2499. [CrossRef]
177. Razola, S.S.; Pochet, S.; Grosfils, K.; Kauffmann, J.M. Amperometric determination of choline released from rat submandibular gland acinar cells using a choline oxidase biosensor. *Biosens. Bioelectron.* **2003**, *18*, 185–191. [CrossRef] [PubMed]
178. Silber, A.; Hampp, N.; Schuhmann, W. Poly(methylene blue)-modified thick-film gold electrodes for the electrocatalytic oxidation of NADH and their application in glucose biosensors. *Biosens. Bioelectron.* **1996**, *11*, 215–223. [CrossRef]
179. Zhu, L.; Zhao, R.; Wang, K.; Xiang, H.; Shang, Z.; Sun, W. Electrochemical behaviors of methylene blue on DNA modified electrode and its application to the detection of PCR product from NOS sequence. *Sensors* **2008**, *8*, 5649–5660. [CrossRef] [PubMed]
180. Tsuruoka, N.; Soto, S.S.; Tahar, A.B.; Zebda, A.; Tsujimura, S. Mediated electrochemical oxidation of glucose via poly(methylene green) grafted on the carbon surface catalyzed by flavin adenine dinucleotide-dependent glucose dehydrogenase. *Colloids Surf. B. Biointerfaces* **2020**, *192*, 111065. [CrossRef] [PubMed]
181. Miller, K.T.; Mruthunjaya, A.K.V.; Torriero, A.A.J. Beyond the Phenothiazine Core: Mechanistic Insights into the Three-Electron Oxidation of Chlorpromazine. *Molecules* **2025**, *30*, 1050. [CrossRef]
182. Kul, D.; Pauliukaite, R.; Brett, C.M.A. Electrosynthesis and characterisation of poly(Nile blue) films. *J. Electroanal. Chem.* **2011**, *662*, 328–333. [CrossRef]
183. Krikstopaitis, K.; Kulys, J.; Tetianec, L. Bioelectrocatalytical glucose oxidation with phenoxazine modified glucose oxidase. *Electrochem. Commun.* **2004**, *6*, 331–336. [CrossRef]
184. Ben-Aissa, S.; Tripathy, S.; Cass, A.E.G. Implantable electrochemical biosensors: Challenges, strategies, and applications. *Curr. Opin. Electrochem.* **2025**, *54*, 101745. [CrossRef]
185. Feldman, B.; Brazg, R.; Schwartz, S.; Weinstein, R. A continuous glucose sensor based on Wired Enzyme™ technology-Results from a 3-day trial in patients with type 1 diabetes. *Diabetes Technol. Ther.* **2003**, *5*, 769–779. [CrossRef] [PubMed]
186. Stanley, M. Analytical Applications of Modified Electrodes. Ph.D. Thesis, Dublin City University, Dublin, Ireland, 1998.
187. Kang, D.; Ricci, F.; White, R.J.; Plaxco, K.W. Survey of redox-active moieties for application in multiplexed electrochemical biosensors. *Anal. Chem.* **2016**, *88*, 10452–10458. [CrossRef] [PubMed]
188. Saleh, F.S.; Mao, L.; Ohsaka, T. Development of a dehydrogenase-based glucose anode using a molecular assembly composed of nile blue and functionalized SWCNTs and its applications to a glucose sensor and glucose/O2 biofuel cell. *Sens. Actuators B Chem.* **2011**, *152*, 130–135. [CrossRef]
189. Saleh, F.S.; Rahman, M.R.; Kitamura, F.; Okajima, T.; Mao, L.; Ohsaka, T. A Simple and Effective Way to Integrate Nile Blue Covalently onto Functionalized SWCNTs Modified GC Electrodes for Sensitive and Selective Electroanalysis of NADH. *Electroanalysis* **2011**, *23*, 409–416. [CrossRef]
190. Komkova, M.A.; Karyakina, E.E.; Karyakin, A.A. Noiseless performance of prussian blue based (Bio) sensors through power generation. *Anal. Chem.* **2017**, *89*, 6290–6294. [CrossRef] [PubMed]
191. Vokhmyanina, D.V.; Sharapova, O.E.; Karyakin, A.A. Ultra-stable biosensor transducer for continuous monitoring. *Biosens. Bioelectron.* **2025**, *286*, 117638. [CrossRef]

Disclaimer/Publisher's Note: The statements, opinions and data contained in all publications are solely those of the individual author(s) and contributor(s) and not of MDPI and/or the editor(s). MDPI and/or the editor(s) disclaim responsibility for any injury to people or property resulting from any ideas, methods, instructions or products referred to in the content.